SKIPPER

E-2641

SPECTRAL DENSITY MEASUREMENTS OF GYRO NOISE

by
Angelo Truncale, William Koenigsberg
Ronald Harris

February 1972

Orbiting Astronomical Observatory

CHARLES STARK DRAPER LABORATORY

MASSACHUSETTS INSTITUTE OF TECHNOLOGY

CAMBRIDGE, MASSACHUSETTS, 02139

E-2641

SPECTRAL DENSITY MEASUREMENTS OF GYRO NOISE

by

Angelo Truncale
William Koenigsberg
Ronald Harris

THE CHARLES STARK DRAPER LABORATORY
A DIVISION OF MASSACHUSETTS INSTITUTE OF TECHNOLOGY
CAMBRIDGE, MASSACHUSETTS 02139

Approved: R. E. Marshall
Associate Director

Approved: R B Woodbury
Deputy Director

ACKNOWLEDGEMENT

This report presents data from various instruments. Since these data were accumulated by the authors at the various manufacturing test facilities, the success of the program would not have been possible without the enthusiastic cooperation of many individuals at the Draper Laboratory, Northrop Corporation and Minneapolis Honeywell. To these individuals we are most grateful:

In particular, John Dieselmen and Bill West who helped arrange the testing at Northrop, and the assistance by Harris Burger during the testing. At Honeywell, Wayne Hodnefield, Gerry Kraus and Rollie Baldwin made our stay very pleasant. George Carlson was indispensable during the integration and testing of their GG 334.

Back at the Draper Laboratory, for their cooperation at FBM, we thank Jack Aronson, Howard Huemmeler and Ernie Portway. Of course, we appreciate the many in Bill Denhard's group who have made that area a second home. Although we did not test their instrument, we did use Minicom's equipment and programming skills. Hank Brainerd and Mark Katz modified and generated computer programs as required to accommodate our need, while interesting and informative conversations with Des McCarthy perfected the data taking and reduction process.

Within our own Skipper Group, particular thanks go to Dick Marshall for his help in defining the original task, his insights, and his encouragements. To Larry Horowitz, thanks for his linearizing the PSD plots, his general analytical support and for writing Appendix B.

The authors are obliged to Dr. W. Vander Velde for his interest, and his time spent reviewing and commenting on the rough draft of this report. Finally, to Tom Huber of NASA we are most appreciative for recognizing the need and providing the funds.

This report was prepared under DSR Project 55-29240 sponsored by the Goddard Space Flight Center of the National Aeronautics and Space Administration through Contract NAS 5-11002.

The publication of this report does not constitute approval by NASA of the findings or the conclusions contained therein. It is published only for the exchange and stimulation of ideas.

E-2641

SPECTRAL DENSITY MEASUREMENTS OF GYRO NOISE

ABSTRACT

Power Spectral Density (PSD) describes the spectral characteristics of noise power in a manner that gives analysts a realistic knowledge of systems component uncertainty and gives the component designer a tool for investigating error sources and mechanisms.

In this report, PSD is used to analyze the outputs of several gyros in the frequency range from 0.01 to 200 Hz. Data were accumulated on eight inertial quality instruments designed and manufactured by the MIT/Charles Stark Draper Laboratory, Nortronics Corporation and the Honeywell Aeronautical Division. The results are described in terms of input angle noise ($arcsec^2/Hz$) and are presented on log-log plots of PSD. These data show that the standard deviation of measurement noise was 0.01 arcsec or less for some gyros in the passband from 1 Hz down to 0.01 Hz and probably down to 0.001 Hz for at least one gyro. For the passband between 1 and 100 Hz, uncertainties in the 0.01 and 0.05 arcsec region were observed.

by Angelo Truncale
William Koenigsberg
Ronald Harris

February 1972

TABLE OF CONTENTS

SUMMARY

As part of the Advanced Orbiting Astronomical Observatory study contract, sponsored by NASA's Goddard Space Flight Center, gyro noise data were accumulated from MIT, Nortronics and Honeywell inertial grade gyros and the spectral characteristics of the noise in the passband from 0.01 Hz to 100 Hz were analyzed. A single instrument from each of the following types was tested: MIT/CSDL TGG viscous integrator, TGG pre-prototype, TGG prototype, 25 IRIG, 18 IRIG and 2FBG-6F-OAO; Nortronics GI-T1B and GI-K7G; and Honeywell GG 334. The instruments were tested at the manufacturer's locations and except for an analogue torque-to-balance loop and magnetic tape recording system required specifically for this test, their electronic support equipment was used. The signal generator output noise was calibrated (and normalized) in equivalent arcsec of rotation about the gyro's input axis and the reduced data is presented as power spectral density ($arcsec^2$/Hz) of this quantity.

Gyro outputs measured and analyzed in this report include not only noise due to sources within the instruments but also noise contributed by the support electronics and base motion. The support electronics are those normally used to support instrument tests by the manufacturers and hence are considered to be legitimate "gyro noise sources" even though it is believed that improved electronics generally would lead to improved gyro performance. On the other hand, angular base motion (which is actually signal interpreted as noise in this, and most tests) is not a legitimate source of instrument noise. In the absence of a means for obtaining direct measurement of angles with standard deviations less than 0.01 arcsec in the 0.01 Hz to 100 Hz passband, test data were accumulated with the gyros at various orientations and also with the wheel off to obtain indirect indications of the possible contribution of base motion. It is possible that up to one-half of the noise reported as gyro noise actually is caused by angular motion; hence, the results reported must be considered conservative.

In the passband from 1 Hz to 100 Hz, the standard deviations measured are as follows: 0.01 arcsec or less for the GI-K7, GG 334 and TGG; approximately 0.04 arcsec for the 25 IRIG and 18 IRIG; and 0.1 arcsec for the GIT-1B and the 2FBG-6F OAO which has a ball-bearing wheel. In the passband from 1 Hz down to

0.01 Hz, the region of primary interest for fine pointing a large space telescope, the standard deviations measured were less than 0.005 arcsec for the GG 334 and TGG, between 0.005 and 0.010 arcsec for the GI-K7G and the 25 IRIG, 0.017 arcsec for the 2FBG-6F-OAO, 0.018 arcsec for the GIT-1B and 0.028 arcsec for the 18 IRIG. It is noted that even though several gyros are competitive from 100 Hz down to 0.01 Hz, the gyros start exhibiting significantly different long-term characteristics as the frequencies are lowered below 0.01 Hz; i.e., as the period of time during which the gyro is depended on for angle information is extended beyond a few minutes. Performance at these frequencies is usually characterized by the long-term drift stability of the instrument; a subject that has received considerable attention from gyro designers, but which is not covered in this report. In fact, the reader is cautioned not to extrapolate the spectral characteristics derived herein to periods longer than one-half hour without corroborative, long-term data. Based on these numbers, it is concluded that gyros can provide attitude information for the stabilization of the large-scale telescope in the passband from 1 Hz down to 0.01 Hz and probably down to 0.001 Hz. Information from optical sensors would be required from 0.01 Hz or 0.001 Hz down to dc.

Additional conclusions reached from this study are:

1. the methods developed in this report provide a very useful technique for obtaining comparative power spectral density information from gyros,
2. the data contained herein provide a rich source of information for both gyro and system designers,
3. efforts should be continued to eliminate angular base motion problems,
4. additional work should be performed to extend the information to frequencies down to at least 10^{-6} Hz.

SECTION I

INTRODUCTION

One of the primary concerns in developing the Advanced Orbiting Astronomical Observatory (OAO) is whether sensor noise will be a limiting factor in controlling the experiment's line-of-sight. Optical requirements dictate that the rms noise level of the telescope pointing angle be constrained to 0.01 arcsec or less. This formidable precision demanded detailed analysis of the spectral characteristics of noise in gyros that could be used in the Advanced OAO. Specific interest is in gyro noise levels with standard deviations of 0.1 arcsec and less in the frequency range from 0.01 Hz to 100 Hz. This spectral information and startracker data can then be used with control system simulations to estimate noise levels that can be expected during fine pointing of the OAO and to determine optimum mixing of star-tracker and gyro data. A further benefit anticipated is the identification of noise mechanisms that could lead to improvements in gyros and associated support equipment.

In the past, spectral analysis has been applied to gyros either to characterize their long-term drift characteristics, i.e., at frequencies less than 0.001 Hz (Ref 5) or to identify specific noise sources generally at frequencies greater than 10 Hz (Ref 6) . To the authors' knowledge, this is the first attempt to obtain data in the mid-frequency range and most likely is the first attempt to obtain comparative data from instruments made by several different organizations. The primary emphasis in developing these tests was to provide meaningful, comparative data. The electronic support equipment, such as wheel supplies, microsyn supplies, and temperature controllers, was provided by each contractor. These electronics were those normally used during the manufacturer's tests and hence were considered to be compatible with the performance level of the instrument. The absolute value of the noise probably is less well defined than the relative values because the contribution of base motion could not be measured directly. Therefore, each gyro was tested in three conditions (output axis vertical – wheel off, output axis vertical – wheel on, and input axis vertical – wheel on) so that possible effects of base motion could be identified. This approach was adequate for this series of tests because it provided a conservative estimate of absolute noise levels. For satellites stabilized with respect to inertial space, these data should be even more conservative because g-sensitive and scale factor terms would be minimal.

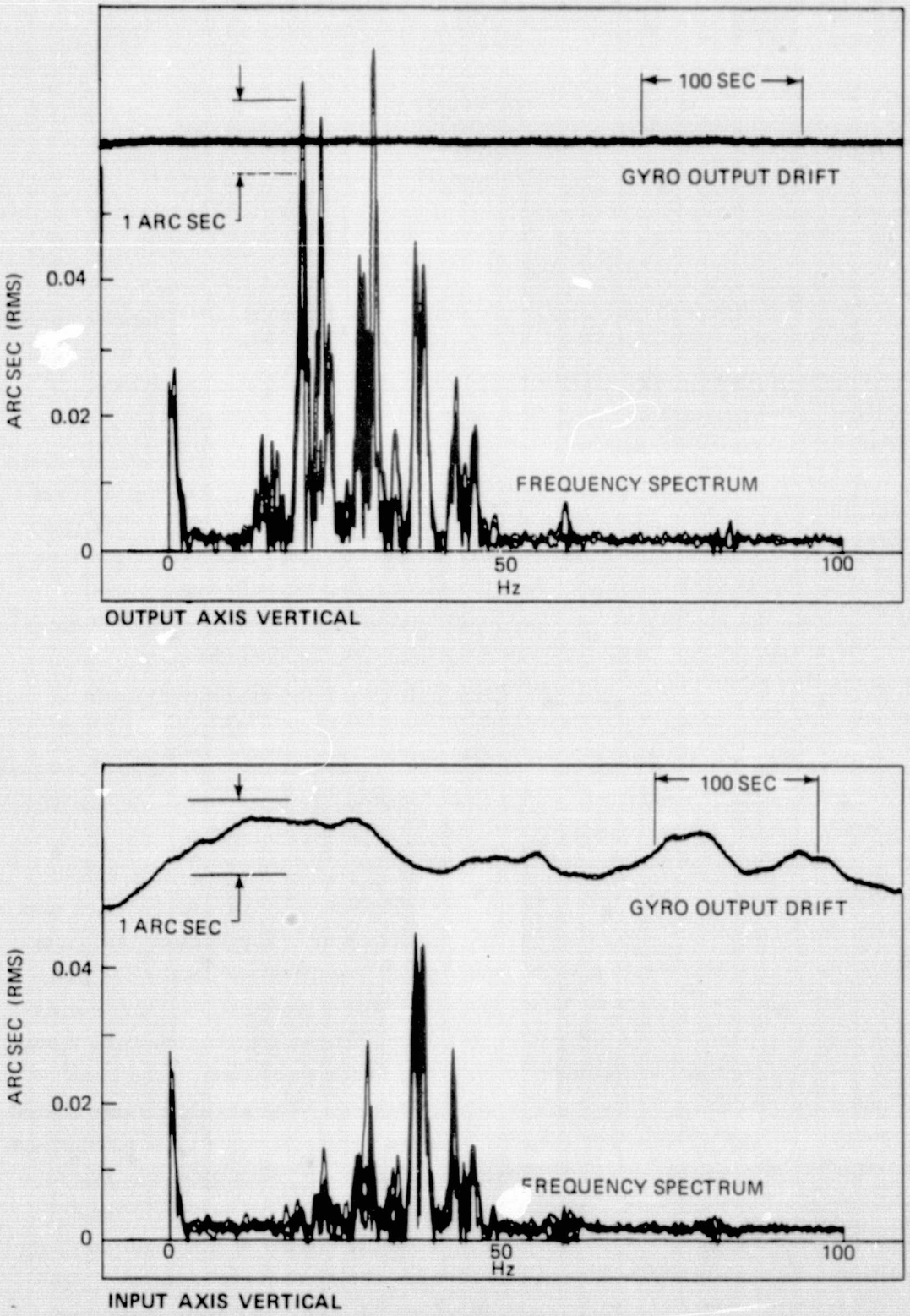

Fig. 1.1 Comparison of Drift and Spectral Characteristics for a Gyro with Output Axis Vertical vs. Input Axis Vertical.

It is emphasized here that the results presented in this report reflect a "one-dimensional" comparison of gyros. The reader is cautioned to recognize that the report does not consider other important factors such as long-term stability (> 1 hr), reliability, size, weight, power, and gain. In this light, one should not be misled into thinking that the quietest gyro is necessarily the best gyro. As previously mentioned, many factors must be weighed when selecting an instrument for a given application. A final caution is that the data were accumulated from one gyro in each design and therefore need not characterize the class.

In evaluating the significance of the random component of drift, which occurs in gyros, it is important to select the proper passband, i.e., establish the frequency range of interest. This is illustrated in Fig. 1.1 where the time histories and corresponding spectral content of gyro angle are presented. The same gyro was used, but the two plots correspond to two distinct orientations. The spectral plots were obtained by employing a commercial wave analyzer whose smallest resolution bandwidth was 1 Hz.* If one had to choose between two instruments based on the time histories of drift shown in Fig. 1.1, the obvious choice would be the one whose output exhibited the smaller average deviation from a nominal value (Fig. 1.1 (a)). This conclusion would differ if the choice were to be based on the spectral plots shown in Fig. 1.1 for clearly, the instrument whose spectral content is smaller at virtually all the frequencies shown is the one whose time history is undesirable.

The resolution of this apparent paradox is of great importance when selecting an inertial sensor for application in the OAO. The problem is solved by recognizing that the resolution bandwidth of the wave analyzer used to obtain the spectral plots in Fig. 1.1 was 1 Hz. Consequently, significant power at frequencies less than 1 Hz are not resolved adequately, and the spectral information obtained below this point has little or no meaning. Mathematical models of noise mechanisms based on spectral information, as shown in Fig. 1.1, will lead to errors in the predicted long-term behavior of the instruments themselves. This example indicates the necessity for resolving spectral components at frequencies well below 1 Hz. Digital techniques provide the means to obtain this fine resolution capability. The Fast Fourier Transform, about which a large body of knowledge and experience has been accumulated in the past six or seven years is the technique best suited to yield the desired information. In order to display spectral density information in the most efficient manner over the frequency range of interest, log-log plots are employed throughout the rest of this report.

*Note that spectral density information is not shown in Fig. 1.1. The wave analyzer produces an rms output with a resolution bandwidth of 1 Hz for a range of frequencies from 1 to 100 Hz.

For practical purposes, high quality inertial gyros may be assumed to be linear time-invariant systems from the point of view of signal transmission. Therefore, when noise sources within the gyro are represented as filtered white noise processes, the spectral density plots exhibit slopes (on log-log paper) that are multiples of 2, e.g., -2, 0, +2, etc. This is a consequence of the properties of rational transfer functions which characterize linear, time-invariant systems.

Breakpoints on these plots reflect the correlation times associated with the filtered noise processes and the dynamics of the instrument as well. If several noise mechanisms are present in a gyro, it becomes difficult to establish their sources. However, knowledge of the dynamics of the instrument in conjunction with spectral density information at the gyro output can lend insight into the nature and source of several internal noise sources and assist with the proper interpretation of the data presented in this report.

For the purposes of this report, we assume that two basic noise sources are present within the gyro. One is a random disturbance torque applied to the float and the other, unrelated to a torque mechanism, is a random process which produces undesired signals in the signal generator. In order that quantization noise be minimized, data were recorded using an analog torque to balance loop with a break frequency below the lowest frequency of interest. In this way spectral measurements of the gyro output closely reflect processes within the gyro itself.

One might conjecture that the feedback control circuitry could introduce noise of its own, thus interfering with the desired measurement. This may well be true, but it is necessary because the rebalance circuitry serves to maintain the gyro float angle about a null position, an essential requirement in the operation of a high quality inertial gyro. However, knowledge of the gyro dynamics and control circuitry is a great aid in deciding where the observed noise comes from.

A simplified block diagram of a gyro is shown in Fig. 1.2, where ϕ_1 refers to the torque noise, and ϕ_2 refers to the angle noise for which a mechanism may exist in the gyro signal generator. Measurements of the angular motion of the float

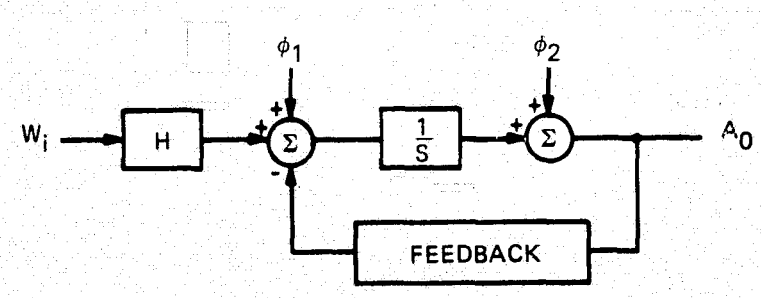

Fig. 1.2 Simplified Block Diagram of Gyro Dynamics.

are recorded for analysis. A fixed feedback gain was selected so that the gyro would behave as a rate integrator over the frequency range of 0.004 Hz to the natural frequency of the float. Over this frequency range, angular motion of the float is proportional to angular motion experienced by the gyro about its input axis. Transfer functions relating the measured output A_o to the noise sources ϕ_1, and ϕ_2 are shown in Fig. 1.3. Note that in Fig. 1.2, angular motion of the float can be

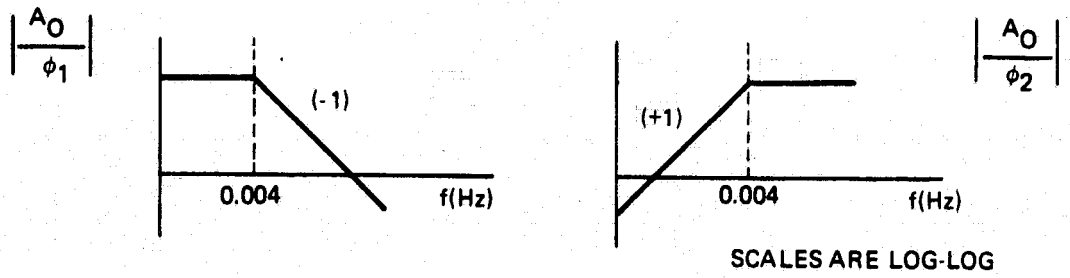

Fig. 1.3

affected by signals entering the gyro through the angular momentum of the wheel, H. Consequently, the PSD of float motion will depend on the angular motion environment in which the gyro is tested. This is an undesirable situation for investigating gyro noise sources, but it emphasizes the need to know something about the power spectral density of ground motion. To assess the possible effect of ground motion, tests were conducted with the wheel on and with the wheel off. Differences in the resulting PSD plots reflect the spectral content due to ground motion, wheel operation, and changes in heat patterns within the float.

There is a scarcity of reliable spectral information characterizing ground motion at the 0.01 arcsec level in the frequency range of interest. The current gyro noise investigation is expected to shed some light in this area. With more exacting gyro requirements, it is likely that reliable spectral information on ground motion will be in greater demand.

This report is divided into six sections and contains four appendices. Results, conclusions and recommendations are presented in Section 2. The support electronics used in conjunction with the gyro tests are described in Section 3. Methods of data acquisition and reduction are discussed in detail in Section 4. The heart of the report is Section 5 where instrument test results are shown. The significance of the minus one slope in power spectral density is treated in Section 6. Additional material of a practical nature is discussed in the four appendices whose titles are shown on the following page.

A. THERMAL NOISE CONSIDERATIONS IN SIGNAL GENERATOR DESIGN.

B. A LINEAR DISTRIBUTED SYSTEM WHOSE AGGREGATE POWER TRANSFER FUNCTION EXHIBITS A MINUS ONE SLOPE.

C. HELPFUL HINTS FOR IMPLEMENTING POWER SPECTRAL DENSITY CALCULATIONS

D. SEISMIC CONSIDERATIONS

For convenience, all references are contained in one list that is located at the end of this report.

All raw PSD plots are available in the Supplement to this report (E-2641) which is published seperately.

SECTION 2

RESULTS, CONCLUSIONS AND RECOMMENDATIONS

The PSD test results accumulated for each instrument are presented in Section 5 as linearized plots that show gyro PSD in terms of slopes, levels and resonances for frequencies between 0.01 and 300 Hz. Because the levels in these plots cover five orders of magnitude, their comparison is difficult and somewhat awkward. For convenience in presenting a comparative summary of the noise characteristics of the various gyros, their PSDs have been converted to the standard deviation of noise in two passbands. The "high" frequency passband covers frequencies from 1 Hz up to 100 Hz (Fig. 2.1). The "low" frequency passband begins at 1 Hz and goes down to frequencies as low as 0.01 Hz (Fig. 2.2). Although these data include noise due to support electronics and base motion, the levels of noise measured are surprisingly low.

The high frequency data show that in the 1 Hz to 100 Hz passband:

1. The gyros with the quietest outputs were the Honeywell GG 334, Nortronics GI-K7G and MIT/CSDL TGG. The standard deviations of noise measured in the high frequency passband were 0.010 arcsec and less.
2. The standard deviations of noise measured in this passband for the MIT/CSDL 18 IRIG and 25 IRIG gyros were approximately 0.045 arcsec.
3. The standard deviation of noise measured on the 2FBG-6F-OAO Ball-Bearing Gyro was 0.115 arcsec, with most of the noise (0.102 arcsec) due to many resonances between 10 Hz and 60 Hz. No rectified bearing noise was observed at frequencies below 10 Hz.
4. The GIT-1B was the noisiest gyro in the high frequency passband. A significant portion of the noise was contained in the resonance at 37 Hz which caused the standard deviation to rise from 40 to 170 milliarcsec.

For data presented as a function of time, a passband is implicit due to the data sampling, data reduction and data presentation methods (e.g., one week of one hour samples). For a PSD presentation, the passband is explicit (e.g., the units are $(\text{arc sec})^2/\text{Hz}$ or $(\text{meru})^2/\text{Hz}$). The standard deviation of noise, σ, in the passband from f_1 Hz to f_2 Hz is defined by the PSD as follows:

$$\sigma^2 = \int_{f_1}^{f_2} (\text{PSD})\,df$$

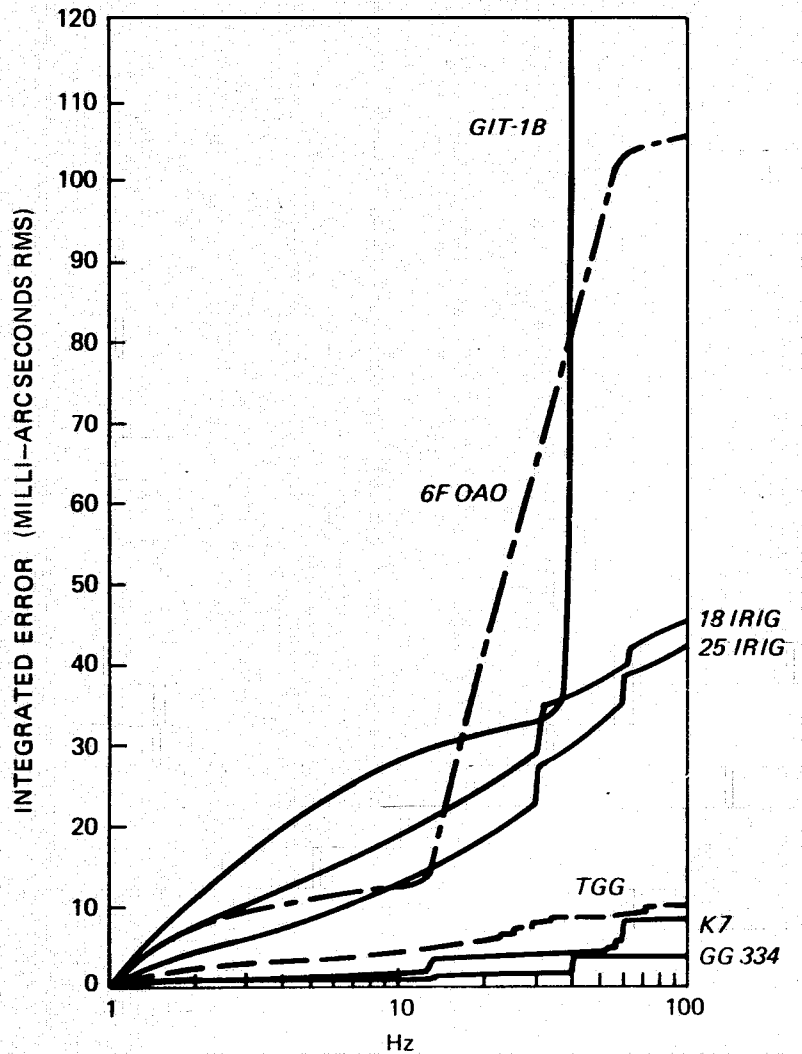

Fig. 2.1 Integrated Error for Passband of 1 to 100 Hz.

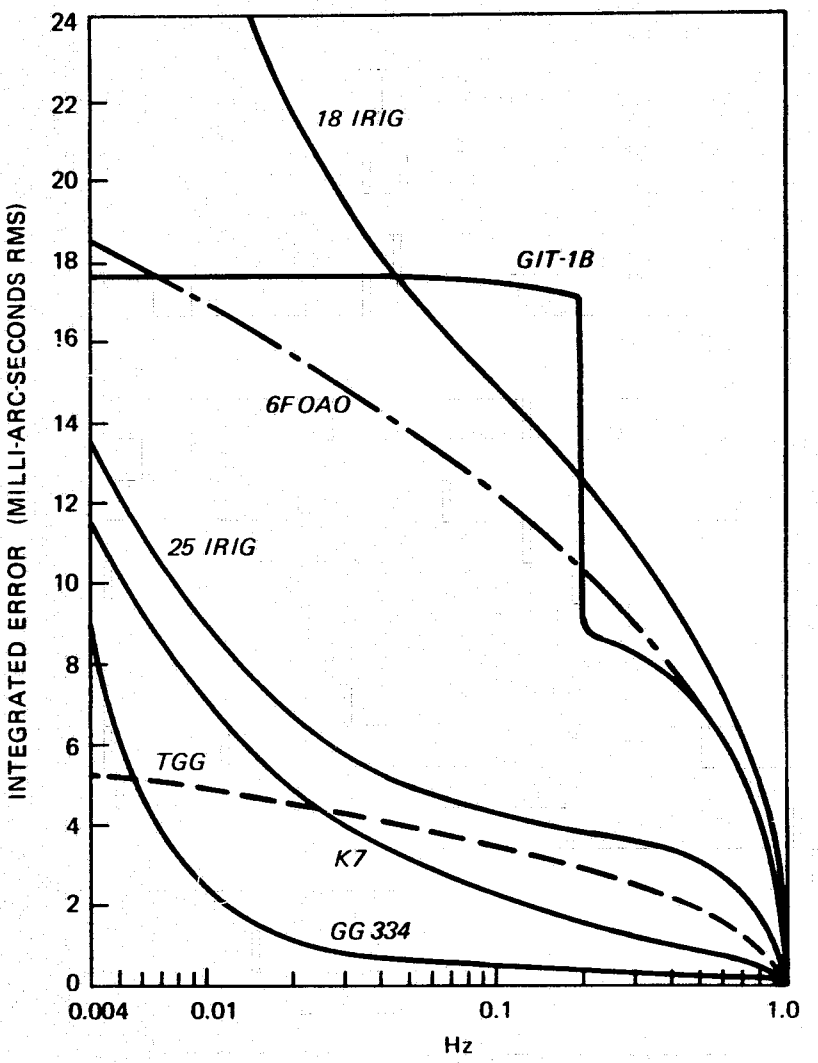

Fig. 2.2 Integrated Error for Passband of 0.01 to 1 Hz.

The low frequency data show not only the noise levels in the 1 to 0.01 Hz passband, but also indicate the rate with which they are expected to change in the next lower frequency decade. For example, if the PSD is proportional to $1/f^2$ at low frequencies, then the standard deviation will be proportional to $1/\sqrt{f}$ or, in terms of time (t), the standard deviation of the noise will increase in direct proportion to $\sqrt{t}$. Extrapolation of these data below frequencies of 0.001 Hz is definitely discouraged.

1. The GG 334 exhibits the lowest noise in the low frequency passband; however, at the 0.01 Hz point its PSD has a slope of minus four so that the standard deviation of noise can be expected to increase directly with $t^{3/2}$. This is consistent with GG 334 long-term performance (~0.1 meru).

2. The standard deviation of the TGG noise is 0.005 arcsec for frequencies down to 0.01 Hz. Its PSD has a slope of minus one so that the standard deviation of its noise can be expected to increase directly with $\sqrt{\ln t}$. Thus, the TGG should provide angle information to at least 0.001 Hz before the standard deviation of its noise exceeds 0.01 arcsec.

3. The standard deviation of noise measured in the low frequency passband for the GI-K7 and the 25 IRIG are below 0.010 arcsec. However, the slopes of their PSDs are minus two at low frequencies so that the standard deviations of their noise can be expected to increase directly with $\sqrt{t}$. Their noise would exceed 0.010 arcsec well above a frequency of 0.001 Hz.

4. The GIT-1B is the only gyro whose data contains a resonance at frequencies below 1 Hz. This resonance contributes 8 milliarcsec of uncertainty; however, because the PSD of the GIT-1B at frequencies between 0.01 and 1 Hz exhibits white noise (zero slope) characteristics, the uncertainty does not increase further with time.

5. The standard deviation of noise for the 2FBG-6F-OAO is relatively high (0.017) at 0.01 Hz. However, the slope of its PSD is minus one so that by 0.001 Hz its performance should surpass all but the TGG gyro.

2.1 Discussion

The data accumulated provide information and insights in three areas:

a. the relative instrument quality in the frequency range of interest,

b. insights into noise mechanisms,

c. further instrument modelling.

2.1.1 Mechanisms

The data presented were accumulated when similar tests were performed on instruments at several test locations. Although the results describe the gyro output characteristics, many questions are raised in regard to the mechanisms responsible for the various noise levels and slopes noted in these results. To avoid jumping to the wrong conclusions these questions must be asked, although the answers are not at hand at this time. For example, base motion vs electronic support vs instrument noise, or lack of noise vs lack of sensitivity, or electrical vs mechanical float suspension system, etc. Comments in the following paragraphs and throughout this report are made from the point of view of systems oriented experimenters and not as experts in gyro or gyro component design. It is hoped, however, the experts may react to the comments and be stimulated by the data.

Mechanisms responsible for the noise recorded may come from within the instrument or be caused by several external sources. Since external sources may account for up to 50% of the noise recorded, these are worth discussing. Prime candidate sources of external noise are base motion and electronic support equipment including excitations, amplifiers, temperature control techniques, etc.

Base motion was a persistent concern throughout the test series. Attempts at independent earth motion measurements with a pendulum met with limited success. However, as more gyro data were accumulated, it was concluded that base motion contributed no more than 50% of the noise. This conclusion was made on the basis that only minor differences exist between gyro data taken with output or input axis vertical or with wheel off. Except for inertia coupling of angular or linear accelerations, wheel—off data cannot contain any angular rate information.

When a minus one slope (in power) appeared in the output of several of the instrument data, mechanisms outside the instruments were investigated. One possibility was flicker noise in the signal generator preamp or data recording equipment. Flicker noise results from microscopic processes on the surfaces of semiconductors. To determine whether flicker noise was causing the minus one slope observed in the data, a test was conducted on the signal generator electronics and data recording equipment with a microsyn secondary as the input load. These data exhibited the characteristics of white noise indicating that this noise source is not a predominating interference in the bandwidth of interest.

The float suspension system in the Nortronics GI-K7 and the Honeywell GG 334 differ from the other gyros tested, and perhaps for this reason their high frequency noise is lower than that of the other gyros tested. While floats in the other instruments are all magnetically suspended, the GI-K7 employs a taut wire to maintain the float centered, whereas a dithered jewel reduces pivot to jewel friction

in the GG 334. The question is whether the magnetic suspension introduces noise or whether these other methods attenuate higher frequencies by tying the float to the case more closely. Additional tests and analysis are required to determine the effect of "total" suspension on higher frequency instrument noise.

Extensive noise studies (Ref 6) by Honeywell on the GG 334 resulted in placing a shroud around the wheel motor to convert turbulent air flow to laminar air flow. Because a similar shroud does not exist in any other instruments tested, turbulence may be at least partially responsible for the higher noise levels.

A further consideration is the overall gain $\left(\frac{H}{C_d} S_{SG}\right)$ of the gyro. Since the recorded output of the gyro was normalized to 1 volt per arcsec of input axis motion, electronic gain was added, as required to achieve this sensitivity. In each case then, any signal generator or electronics noise is weighted by $\left(\frac{C_d}{H S_{SG}}\right)$. This simple signal-to-noise relationship can be best appreciated by noting the strong correlation, evident in the following figure, between the standard deviation of noise in the 1 Hz to 100 Hz passband and the gain of each instrument.

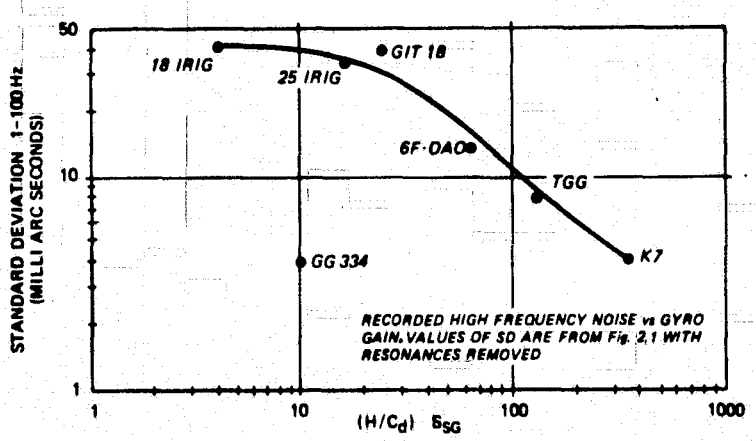

No particular correlation seems to exist between gain and uncertainties below 1 Hz:

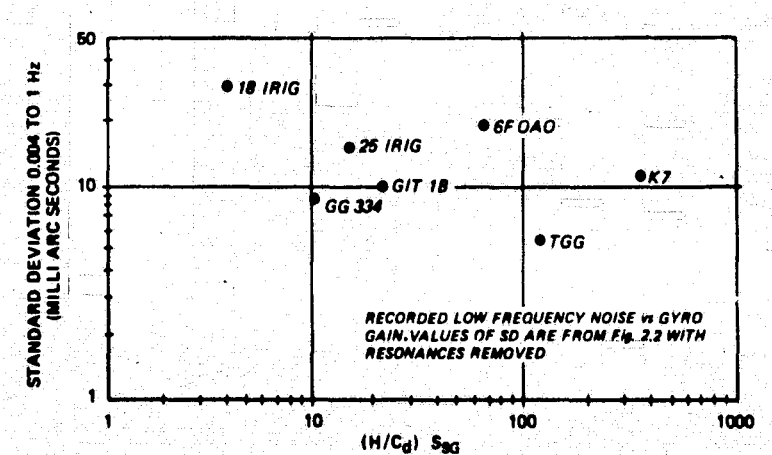

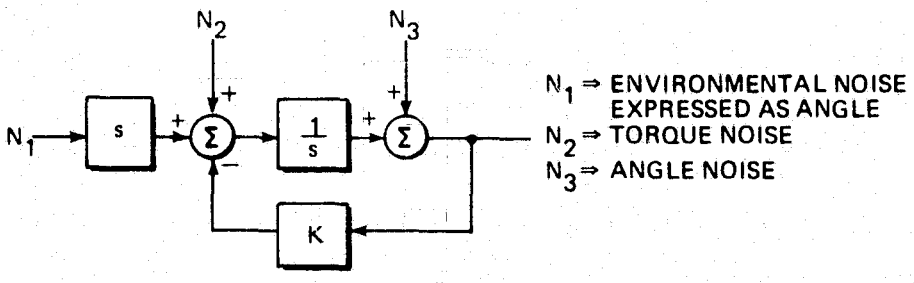

MODEL	SPECTRAL CHARACTERISTICS at INPUT	SPECTRAL CHARACTERISTICS at OUTPUT (POWER)
WHITE ANGLE NOISE N_3	(0) CONSTANT POWER DENSITY	(+2) $\frac{1}{\tau}$
MARKOV ANGLE NOISE N_3	EXPONENTIALLY CORRELATED RANDOM PROCESS $\frac{1}{\tau_m}$	$\frac{1}{\tau}$ (-2) $\frac{1}{\tau_m}$
WHITE TORQUE NOISE N_2	(0) CONSTANT POWER DENSITY	(-2) $\frac{1}{\tau}$
MARKOV TORQUE NOISE N_2	(0) EXPONENTIALLY CORRELATED RANDOM PROCESS (-2) $\frac{1}{\tau_m}$	$\frac{1}{\tau_m}$ (-2) $\frac{1}{\tau}$ (-4)
RANDOM WALK TORQUE NOISE N_2	VARIANCE PROPORTIONAL TO TIME (-2)	(-2) $\frac{1}{\tau}$ (-4)
CONSTANT POWER PER DECADE N_3	(-1) SEE APPENDIX B	(+1) (-1) $\frac{1}{\tau}$

DATA PASS BAND

Table 2.1 Summary of Gyro Noise Models.

2.1.2 Instrument Modelling

Several models have been proposed to describe the behavior of a gyro's output. Generally, these models are described as a relationship between torque or output angle and frequency in the form of the now familiar log-log plot. The characteristics of the more popular models are summarized in Table 2.1. Although efforts are underway to extend PSD measurement to the 10^{-5} Hz region, the data accumulated to the 0.01 Hz frequency fit some of the models shown. With additional data a model or perhaps a model for each category of gyro may emerge.

One of the more interesting noise characteristics observed was a minus one slope in power in the data from the TGG, Viscous Integrator, 2FBG-6F-OAO, and the 18 IRIG. The appearance of this slope caused some doubt about the validity of the techniques used, because slopes in power were expected to be even integers only; however, it was determined that this noise was indeed a part of the gyro noise.

2.3 Conclusions

The data were taken with the knowledge of unequal test conditions. Nonetheless, the test methods appear to be sound approaches to comparing instruments and determining some of their error mechanisms. Some conclusions drawn from the results of the test program with particular reference to the Advanced OAOs 0.01 arcsec stabilization application are:

1. Gyros with ball-bearing wheels are probably too noisy for servos with natural frequencies above 0.1 Hz.
2. The TGG should provide satisfactory angle information for the passband between 0.001 and 1 Hz.
3. The low frequency characteristics of the other gyros tested do not appear satisfactory for advanced OAO use if the frequency of interest is extended below 0.01 Hz.
4. Generally, all the gyros tested are very fine angle transducers.

These conclusions are conservative and made with the realization that if operation in space differs, it should be quieter than operation on the ground. The accumulation of spectral data has provided and is continuing to provide a rich source of information upon which to model gyro error sources. Since in the case of each gyro tested the PSD slopes generated were consistent with the long-term behavior of the instrument, it is apparent that PSD should become a valuable, generally accepted method to describe and evaluate gyro performance.

2.4 Recommendations

As a result of this study, the following recommendations are made:

1. In view of the fact that conservative data have been obtained that show the TGG gyro capable of providing angle information with standard deviations of 0.01 arcsec or less down to 0.01 Hz and probably down to 0.001 Hz, planning for the Advanced OAO's fine pointing loop should include a gyro until similar data has been obtained from a star tracker to show that satisfactory bandwidth and noise levels can be achieved.
2. That work continue to identify noise sources, particularly base motion.
3. PSD be included as an accepted gyro test and that test methods be standardized so that data obtained from different gyros at different locations can be compared.
4. A comparative study of star trackers should be performed to close the Advanced OAO guidance and control question.

SECTION 3

GYRO TEST ELECTRONICS AND TECHNIQUES

The gyro test electronics and techniques were devised to normalize the test situation and reduce error sources in the extraction of instrument noise. Throughout this report, the results are attributed to instrument/environment, where the environment includes both base motion and the characteristics of the electronic support equipment used. As the various circuits and techniques employed are described, error sources which were considered during the course of the program are also discussed. Undoubtedly, some error sources may have escaped us; hopefully, their impact is of little consequence to the published results.

3.1 Test Electronics

The test console* at each location was used to support all gyro functions except the torque-to-balance loop. Connectors in series with the station's gyro connectors permitted the interface of an Analogue Torque Loop package designed for this program. This package shown in Fig. 3.1 performed the functions shown in Fig. 3.2. These functions include an analogue torque loop with the capability of supporting electromagnetic or permanent magnet torquers, signal generator gain and demodulator circuits to provide a normalized readout gain of 1 volt per arcsec, torque and quadrature compensation networks and potentiometers, and provisions for adapting the loop to the parameters of the particular instrument.

3.1.1 Torque Loop Characteristics

The torque loop provides gain between the signal generator (SG) and torque generator (TG) such that the loop can be characterized as a first-order system with a 40-second time constant. This characteristic time was selected because the program's interest was in measuring gyro noise in angle rather than torque. The 40-second characteristic time permits frequencies greater than 0.004 Hz in the signal generator output to be recorded unaltered; whereas, the effects of torque at frequencies less than 0.004 Hz are attenuated with a frequency roll off of -20 db/

*The test consoles were supplied by the vendors and were the consoles normally used for their tests.

Fig. 3.1 PSD Program Hardware - Torque loop with preamp and interface cables.

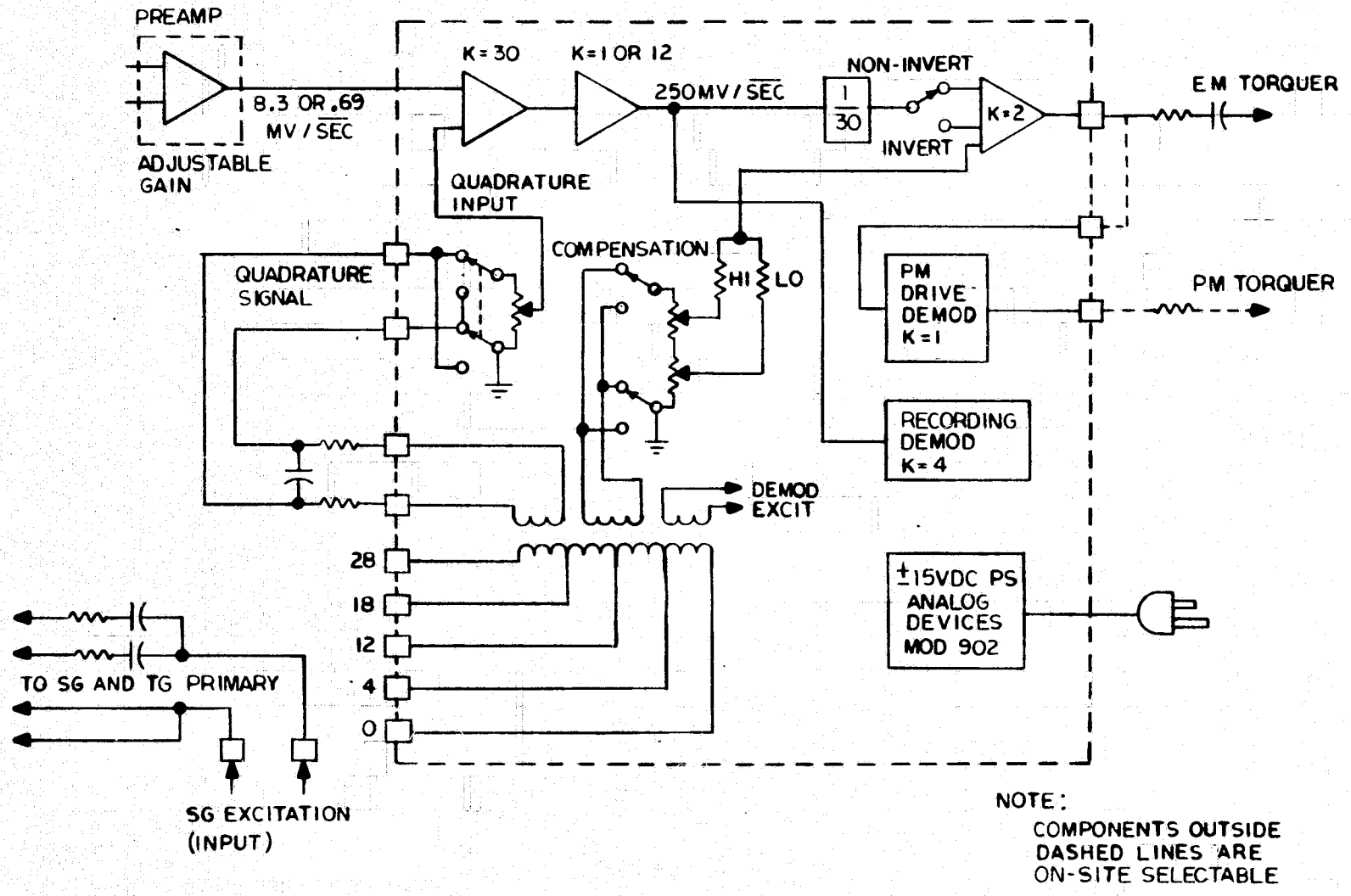

Fig. 3.2 Analogue Torque Loop Electronics.

decade. Because the resulting loop gain is only 1.6 meru/arcsec, parallel torque compensation was provided to permit all data to be accumulated with the SG signal near null regardless of gyro input axis torque.

The data's upper frequency limit was set at 200 Hz by placing a second-order 200-Hz filter at the demodulator output. This filter reduces high frequency fold-over in the PSD extraction. The signal recording bandwidth, in angle, is;

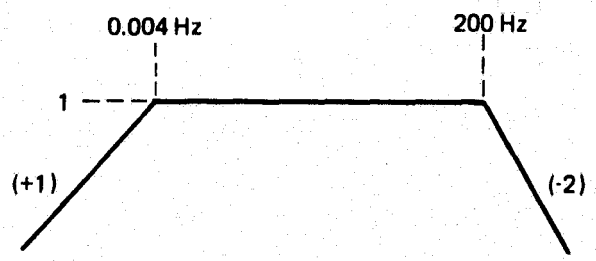

3.2 Integration at Each Facility

Since all the gyros were functionally the same, only minor differences affected torque loop integration at each facility. These differences were:

Permanent Magnet vs Electromagnetic Torquer
Signal Generator Excitation Voltage and Frequency
Signal and Torque Generator Sensitivities

These differences were anticipated and a section of circuit board was provided with pins to enable the "programming" of each situation.

The amplified SG error signal (plus the torque compensation signal) is used to drive the secondary of an electromagnetic (EM) torquer. For a gyro with a permanent magnet (PM) torquer, this signal is demodulated to provide the torquing current.

The SG excitation, from the test console, is used to provide SG primary current, and also to generate quadrature and torque compensation signals, demodulator drive voltages and, as required, to provide TG primary current in an EM torquer. Since the excitation levels encountered at the various facilities were from 4 to 28 volts at frequencies from 1.6 k to 7.6 kHz, a wide band transformer with several input voltage taps was designed to accommodate all situations. The input tap arrangement shown below permits the required excitations to be developed regardless of input voltage level:

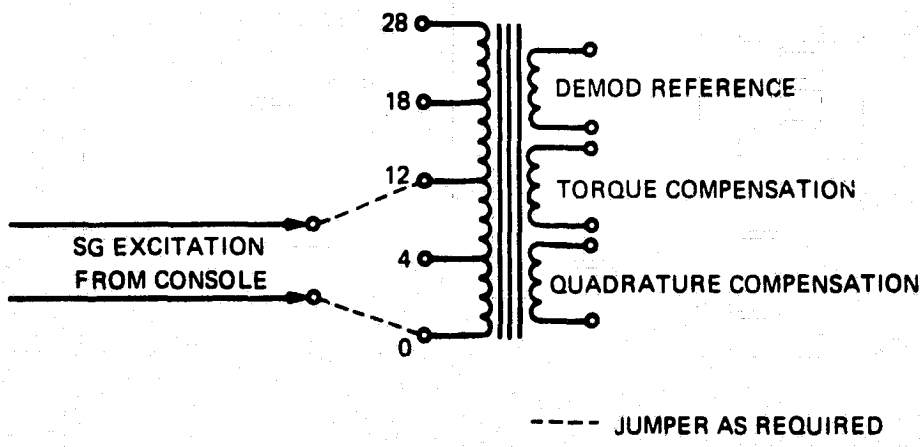

3.2.1 Signal Generator Calibration

The desired 1 volt/arcsec recording sensitivity was achieved by adjusting the gain of two amplifiers. The gain of the second servo amplifier was switch selectable (1 or 12). The preamplifier gain was adjusted (5 to 30) to set the final value which was calibrated as follows. The 1 volt/arcsec sensitivity, in terms of input axis motion, was calibrated open loop against the horizontal component of earth rate. That is, with a known input rate, the time required to traverse a set output voltage was measured:

$$\text{Sensitivity} = \frac{1}{\omega_{ieh} \sin \alpha \text{ (arcsec/sec)}} \times \frac{1}{T \text{ (sec)}} \times V \text{ (volts)}$$

where,

α = ± angle off of east

ω_{ieh} = horizontal component of earth rate

T = time measured

V = set voltage swing

To eliminate any bias or angle (α) errors the operation was performed at both plus and minus α.

This approach calibrated output to input directly and did not require any prior knowledge of angular momentum, damping, signal generator sensitivity or any electronic gains. With nominal values of 2°, 26 seconds and 10 volts the sensitivities to measurement inaccuracies are:

0.8%/arcmin
5.6%/sec
14%/volt

A possible source of error in this calibration method is elastic restraint torque. The % error contributed by this torque is described by:

$$\frac{(E)\beta}{\beta} = \frac{K_R^2 \beta^2}{3\omega_o^2}$$

in which

β = angle (± swing) = ±5 arcsec

K_R = elastic restraint

ω_o = earth rate input ≈ 25 meru

Even for the largest restraint of 1 meru/arcsec, the calibration error is approximately 0.05%, not a significant interference.

Finally, the Q at which the SG is tuned affects the bandwidth of the output signal. The components associated with SG secondary tuning during this test program were as shown below.

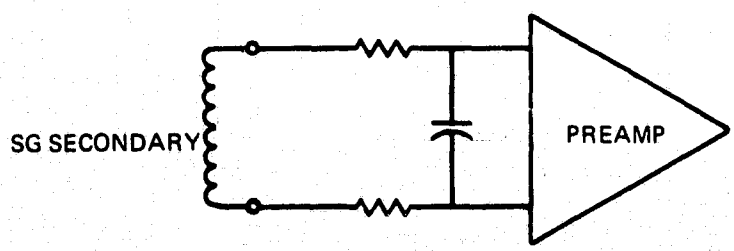

Although the bandwidth varied with each instrument, depending on signal generator parameters and the value of drive frequency, in no case was it below 800 Hz.

3.2.2 Torque Loop Gain Adjustment

Whereas the SG amplifier gains adjust the recording sensitivity, torquing currents are adjusted to give the fixed TG scale factor required to set the loop gain. This gain was adjusted such that the torque loop response to a step input exhibited a 40-second time constant. Physically, it was done in one of two ways. The maximum current capability of the final torque loop amplifier was approximately 5 ma (ac) and 7 ma (dc). In the case of gyros with electromagnetic torquers, the primary current was adjusted to provide the necessary sensitivity. For permanent magnet torquers, the sensitivity was adjusted by setting the value of a resistor in series with the torquer winding.

3.3 Torque Loop Noise

Analysis was performed to determine the relationship between recorded noise and possible noise introduced by the signal generator and torquing circuits. In the normalized situation these two noise sources are introduced in the loop as shown below.

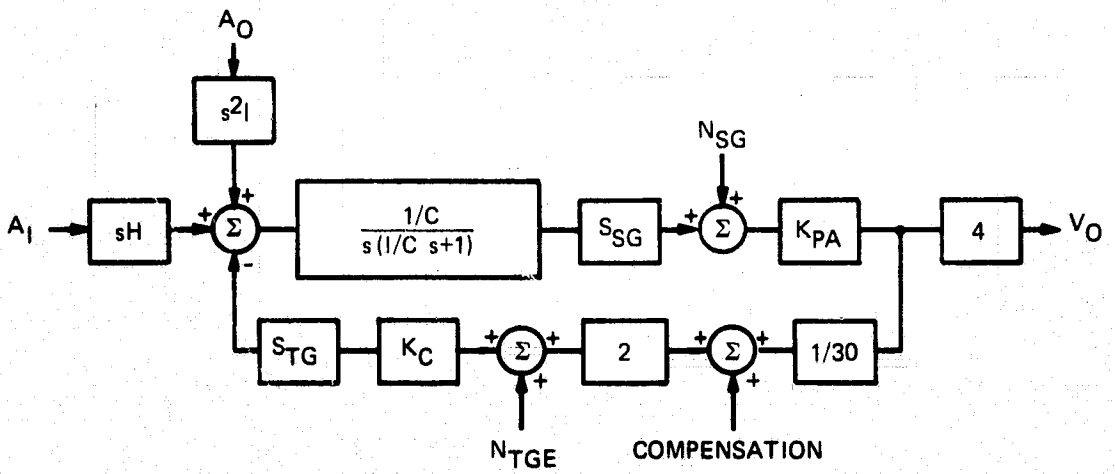

K_{PA} adjusts V_o/A_I = 1 volt/arcsec (open loop dc gain) and K_C is adjusted to set the loop characteristic time at 40 seconds. Because the transfer parameters $\left(\frac{H}{C_d} S_{SG}\right)$ vary between instruments, K_{PA}, and therefore the magnitude of noise in the output, V_o, also varied with each gyro. Any signal generator noise, between the torque loop's cutoff frequency (0.004 Hz) and the natural frequency of the instrument, will be amplified by the gain required to bring $\left(\frac{H}{C_d} S_{SG}\right)$ to 1 volt per arcsec. This noise transfer for the various gyros is:

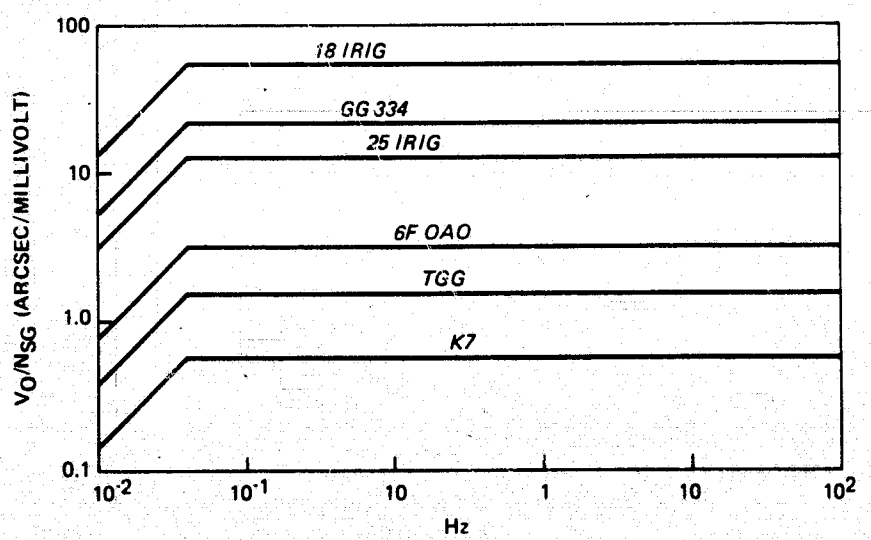

While the effect of SG noise, N_{SG}, varies with K_{PA}, the analog torque loop noise is a constant for all the instruments. The transfer function of V_o/N_{TG}, is

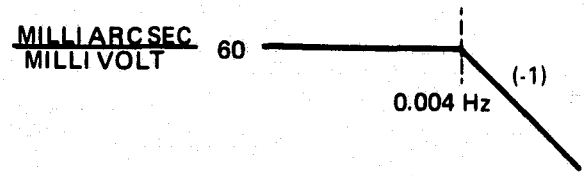

The minus one slope results in a minus two slope in power. The sensitivity of 60 milliarcsec/mv is high; but, since it affects each gyro equally, this noise can be no higher than the lowest instrument value recorded.

3.4 Magnetic Tape Recorders

In the course of the program three tape recorders were used. During initial investigations of procedures and techniques, an Ampex FR 1800L tape recording system was used. This is a high quality rack mounted recorder which was made available by the Draper Laboratory Miniature Components Group.

Portable tape recorders were not available in the Laboratory and therefore, had to be rented. A Bell and Howell VR 3360 initially acquired was later replaced with an Ampex FR 1300. The FR 1300 has a crystal controlled phase-locked speed control whereas the VR 3360's speed is controlled by the 60 cycle line frequency. The characteristics of the three recorders are summarized in Table 3.1. To establish the magnitude of noise contributed to the data by the recording electronics, a set of PSD data with shorted input was accumulated and reduced for each of the portable recorders. The linearized version of the data are shown in Fig. 3.3. The actual PSD plots may be found in the Supplement to E-2641. Although the amplitude content is well below the levels recorded in the gyro data, some of the recorder peaks are detectable in the quieter gyro plots. The minus one slope observed over a portion of the recorder PSD suggests that its origin is due to some magnetic phenomenon.

3.5 Wave Analyzer

An instrument which proved to be a great help in the test program was a Quantech Mod 304 Wave Analyzer. Used with an X-Y plotter, the Wave Analyzer provided an opportunity to record the rms noise content in the signal generator output before it was recorded on magnetic tape. The recording parameters for the

wave analyzer plots included in the Supplement were:

Frequency Range	1 - 100 Hz
Averaging Time	<0.1 seconds
Passband (window width)	1 Hz
Time per Sweep	180 seconds

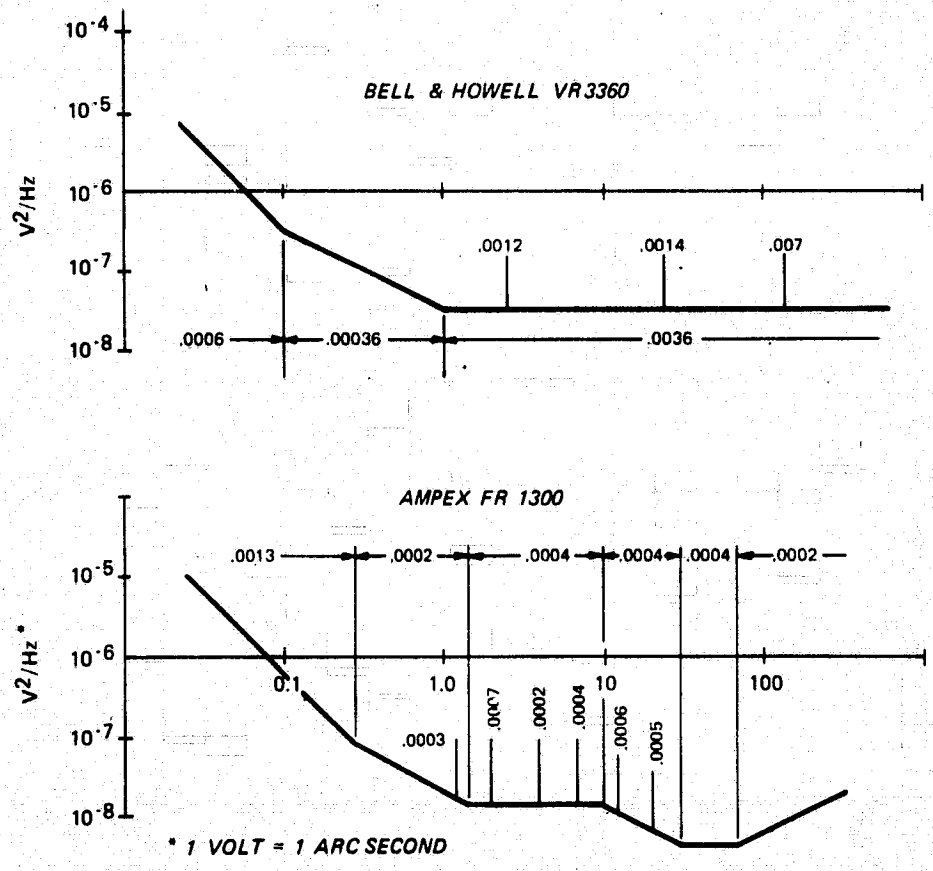

Fig. 3.3 Linearized PSD Results - Portable Magnetic Tape Recorders.

TABLE 3.1

COMPARISON OF TAPE RECORDER SPECIFICATIONS

SPECIFICATIONS @ 30 ips	FR 1800	FR 1300	B & H 3360	
SPEED VARIATION (%)	< 0.25	0.25	60 Hz DEPENDENT	
CAPSTAN SPEED ACCURACY (%)	± 0.05	0.05	± 0.25	
FLUTTER (% p - p)	0.2	0.4	0.35	0.55
FLUTTER BANDPASS (Hz)	0.2-5 K	0.2-5K	0.2-312	0.2-5K
FM FREQUENCY RESPONSE (Hz)	DC-10 K	DC-10K	DC-10K	
RMS S/N RATIO (db)	48	46	45	
FM VOLTAGE LINEARITY (%)	± 0.75	± 0.75	± 0.5	
DC DRIFT (%)	< ± 0.5	< ± 0.5	< 1.0	

SECTION 4

DATA ACQUISITION/REDUCTION

As has been stated previously, the frequency range selected for spectral analysis of the gyro output was from 0.01 to 100 Hz. Commercial wave analyzers capable of investigating frequencies below 1 Hz were not available, so digital computer techniques were used to analyze the entire range of interest. The steps followed in recording and reducing the inertial instrument data are described next. The demodulated error signal from the signal generator was converted to an FM signal and recorded on tape in analogue fashion. The recorded signal was played back into a counter operating in the continuous "time per events" mode. The BCD (Binary Coded Decimal) output of the counter, operating at a nominal rate of 600 samples per second, was placed on magnetic tape by a PDP-8 computer. The PSD analysis of the data on this tape was performed by the Draper Laboratory's IBM 360 computer. The complete sequence is summarized functionally in Fig. 4.1. Note in Fig. 4.1 that an analogue filter was employed before the signal was recorded on tape. This reduces aliasing (spectral folding) which occurs when signals are sampled.

The workability of the method was verified by a series of tests which exercised the entire process. The results of these tests and additional details of the procedure are given in the following paragraphs.

4.1 Tape Recorders

The tape recorders used were capable of operating in two distinct modes. These modes are best described as direct and FM. The direct mode records the input signal directly. This mode is very effective in recording high frequency data but cannot record dc. For example, at 30 inches per second, the direct recording bandwidth is 150 to 150 kHz. In the direct reproduce mode, whatever is on tape is played back directly.

In the FM mode (record), at the 30 ips speed, the amplitudes of those signals in the frequency range dc to 10 kHz are converted to a frequency and recorded. The equation below expresses this conversion.

$$\text{Frequency out} = \text{Voltage} \times \text{Sensitivity (Hz/volt)} + \text{Center Frequency}$$

In the FM mode (reproduce), these frequencies are converted back to an analog signal by electronics in the recorder. The FM mode which has the advantage of recording and reproducing signals with dc and low frequency components, was used to evaluate the record and playback capabilities of the recorder. To determine whether the recorder modified or distorted the input signal, a wave analyzer in conjunction with an X-Y plotter was used to analyze a signal with known frequency characteristics. An example of frequency analysis of a signal generated directly and from a recorder playback of the same signal is shown in Fig. 4.2. The traces of Fig. 4.2 were recorded with equipment arranged as shown in Fig. 4.3. The 15% amplitude reduction in the frequency content of the playback signal is a consequence of the attenuation required to adjust the input signal to lie within the linear range of the FM electronics. Since the maximum input and playback voltage is ±1 volt, record/reproduce gain factors are adjusted accordingly. For data which is computer reduced, the recorded FM signal is calibrated directly in kHz/volt using a reference dc voltage. Similar tests were conducted to confirm that the recorder faithfully reproduced signals at lower frequencies.

4.2 Computer Data Reduction

The first step in the reduction of the recorded data is to measure the time, for a preset number of events (pulses) to occur, with a counter and place the BCD output on magnetic tape using a PDP-8 computer. That is, the amplitude of each sample is determined and stored as a BCD number proportional to the time elapsed during which a fixed number of events occur. The "time per events" mode was selected for two practical reasons. First, continuous data that is necessary for spectral analysis is provided and second, microsecond quantization is realized.

Because the input signal is recorded at a frequency in the range 54 kHz ±21 kHz, a "preset" of 80 events was selected, i.e., the time per 80 events (pulses) was measured. This value assures that at the lowest input frequency (33 kHz), the counter output does not go below a rate of 400 samples per second. This sample rate and the 200 Hz analogue filter preclude significant aliasing into frequencies of 100 Hz or less.

With the preset set at 80 events, the nominal measured time was 1.481 msec. It is clear that in the "time per events" mode, the quantization is 1:1481 while in the "events per time" mode the quantization would be 1:80. Thus, use of the "time per events" mode reduced the "granularity", due to data sampling, of the curve analyzed by the computer.

There is, however, one major disadvantage in recording time rather than events: the samples recorded are not equally spaced in time. This presents a problem since power spectral density analysis using the Fast Fourier Transform

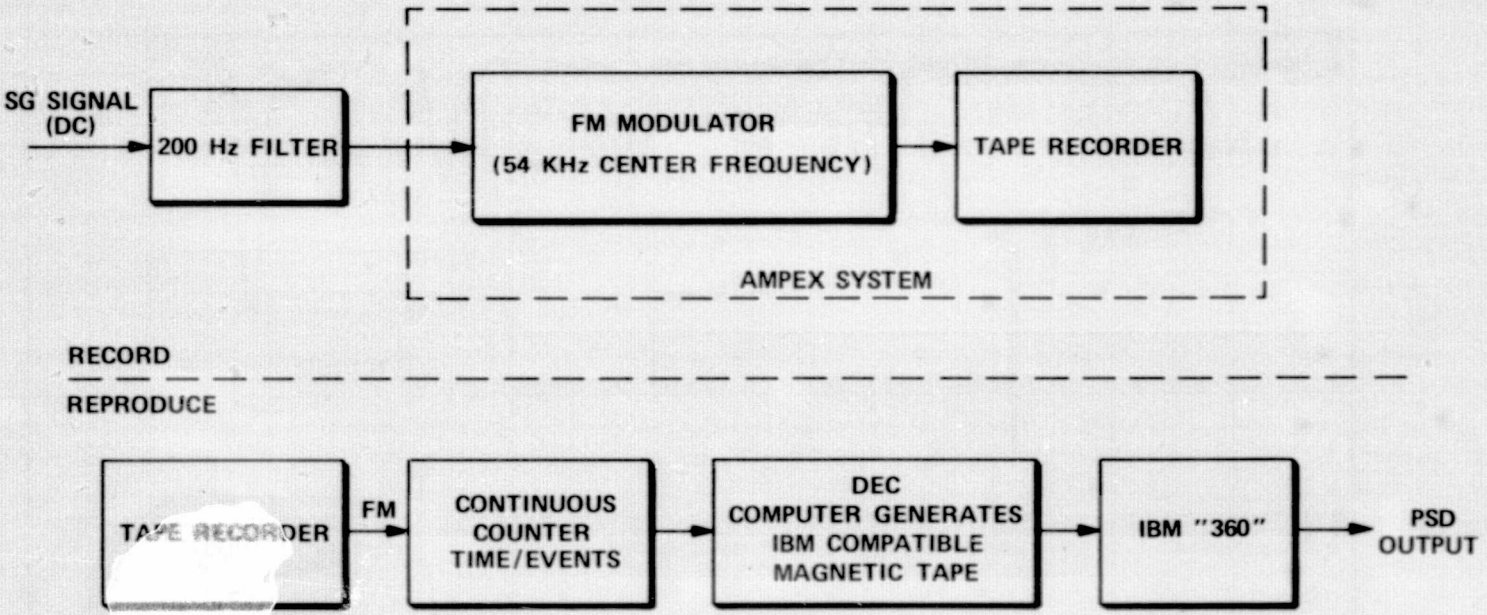

Fig. 4.1 Signal Flow Diagram for Data Recording / Reduction Method.

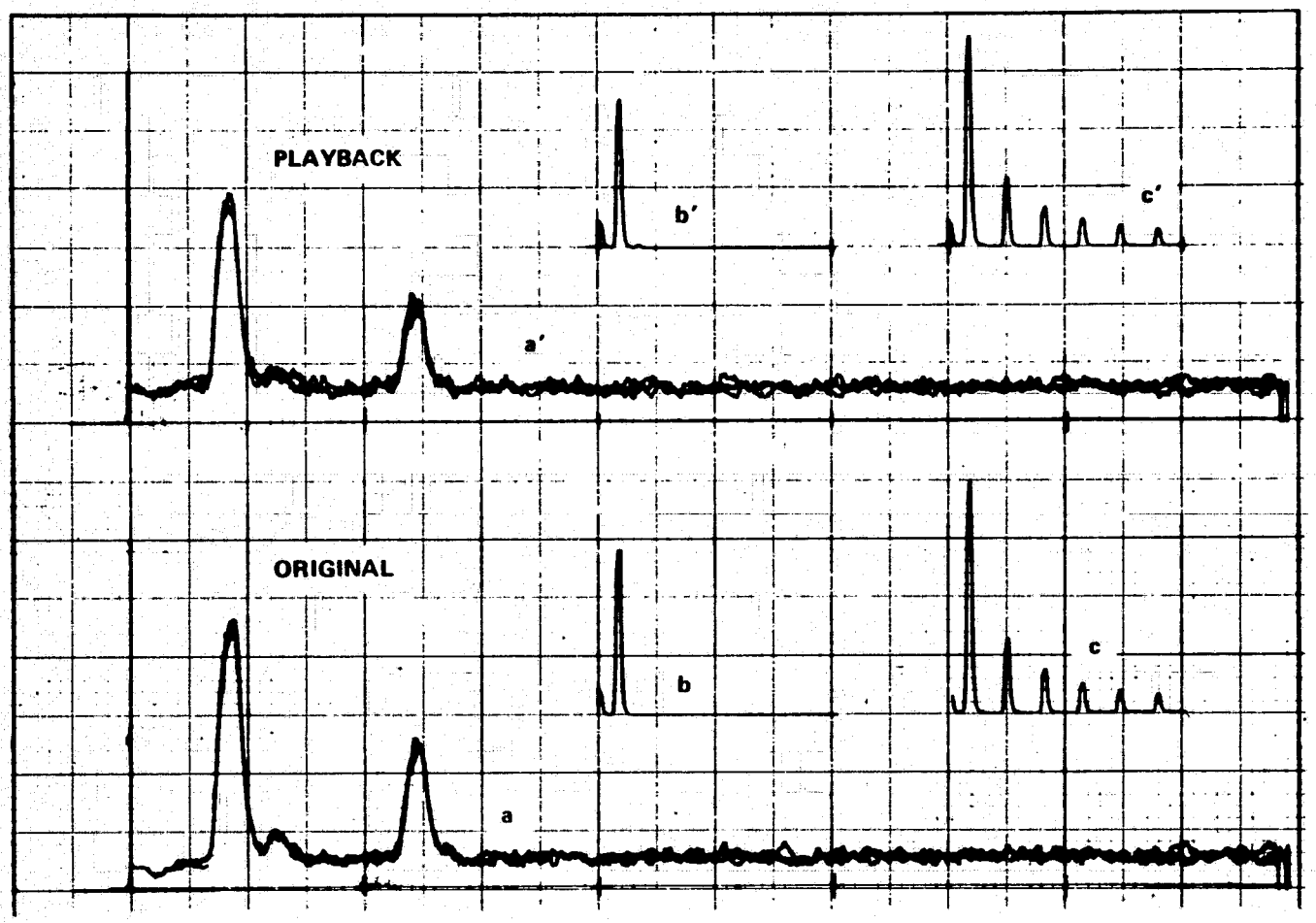

Fig. 4.2 Wave Analyzer Traces of Original Signals and Magnetic Tape Playback.

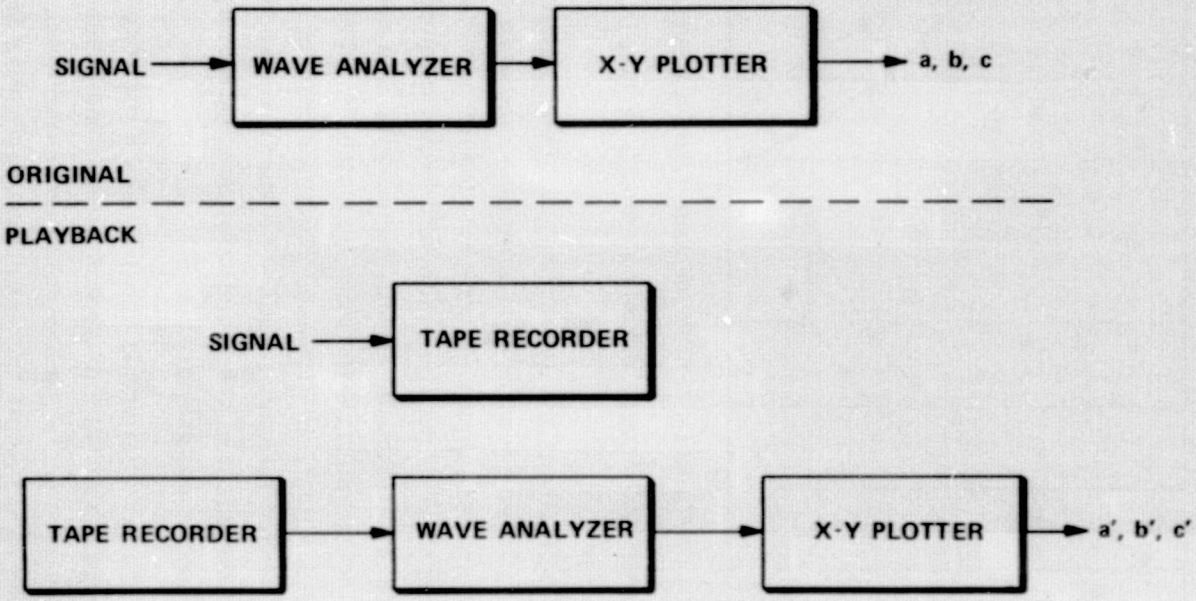

Fig. 4.3 Arrangement Used to Check Tape Recorder's Ability to Reproduce Noise.

requires equally spaced samples. To remedy the difficulty, the first operation performed was to construct equally spaced data using the technique illustrated in the diagram below where some nonuniformly spaced data are modified to produce uniformly spaced samples. The technique is referred to simply as a holding process.

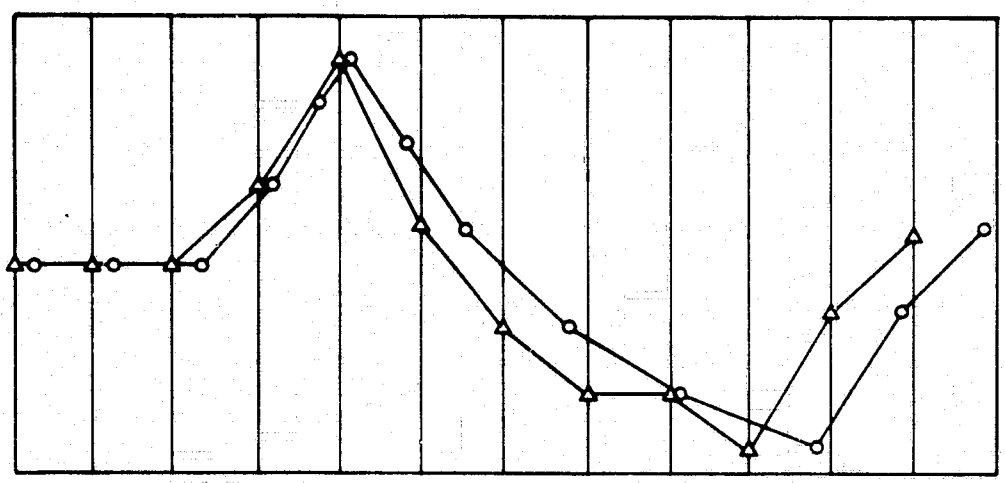

o *ORIGINAL DATA UNEQUALLY SPACED IN TIME (TIME ∝ LEVEL)*

Δ *DATA AFTER APPLYING HOLD - EQUALLY SPACED IN TIME*

While several other conversion methods for generating uniformly spaced data were available, this technique was chosen because of its simplicity and ease of digital implementation. This particular technique produces some nonlinear distortion due to the variation in the "holding time". By using data with known frequency characteristics (square wave) it was shown that the attendant distortion was not significant for our application because the nonuniformities were less than 3%. This was achieved by comparing frequency analysis with and without the holding process. In other applications, it is possible that this frequency distortion may present a significant problem; this and the effect of other methods for constructing uniformly spaced data are currently under investigation.

After generating the required uniformly spaced data, a computer file is produced which contains approximately 20 minutes of information in the units of arcsec. The Fast Fourier Transform, a mathematical technique which extracts frequency components, is performed on 16,384 sequential data points from the computer file. For a nominal sample frequency of 600 samples per second, these 16,384 data points limited the spectrum to a passband ranging from 0.3 Hz to 300 Hz. To extend the frequency range on the low end, a second computer file was created in which the original data was averaged in groups of twelve. In order to minimize aliasing of high frequencies, a 25 Hz, 3^{rd} order, low pass Butterworth filter, implemented digitally, was applied before the averaging was performed.

4.2.1 The Fast Fourier Transform

After the two files were generated, each underwent the same data reduction process resulting in a high and low frequency set of data. Before the Fast Fourier Transform was performed, however, points exceeding 3 sigma from the mean were replaced by the mean after which the recalculated mean and trend were removed from the data. These operations were performed for the reasons outlined below. Points exceeding 3 sigma (standard deviation) from the mean of the time series were replaced by the mean to guard against possible errors in the recording and playback of data that had been prevalent with previous users. Except for data obtained from the pendulum and ball-bearing gyro, no more than 20 points out of 16,384 in any one run exceeded the 3 sigma limit. The mean and trend of the time series, if either exists, are removed because their presence would only serve to distort the power spectral density analysis. This is true because the frequency content of both these terms is already known and it is primarily the frequency content of the random processes occurring within the inertial instrument that are to be ascertained.

A detailed description of the Fast Fourier Transform can be found in several good references, e.g., Rader and Gold (Ref 7), Jenkins and Watts (Ref 8) and Blackman and Tukey (Ref 9). The essence of the technique is to extract the coefficients of a specified number of frequency components of a given time series. This is not a simple task and requires sophisticated numerical techniques to reduce computation time, particularly when a large number of data points require analysis. Several digital filtering methods are employed in conjunction with FFT to reduce what is termed "leakage" (a consequence of the fact that only a finite amount of data may be analyzed).

For our application, 8193 frequency components are extracted from the 16,384 original data points. These range from one-half the original sample frequency down to the original frequency divided by 16, 384.

4.2.2 Condensing and Plotting the Spectrum

The 8193 Fourier coefficients are equally spaced over four decades in frequency and have amplitudes covering up to six orders of magnitude. To condense these data into a reasonable presentation, the discrete power spectrum points are averaged in 1/12 octave steps by successively doubling the number of points averaged as shown in the table below. This reduces the number of data points from 8193 to 151 which are identified as "condensed" data.

Original Data Point	No. of Points Grouped Per Plotted Point	Condensed Data
0-7	-	-
8-31	1	0-23
32-63	2	24-39
64-127	4	40-55
128-255	8	56-71
256-511	16	72-87
512-1023	32	88-103
1024-2047	64	104-119
2048-4095	128	120-135
4096-8191	256	136-151

It should be realized that the price paid for obtaining a clean presentation is a distortion of frequency spectrum. The analysis of white noise illustrates the nature of the distortion (see Fig. 4.4). Note that as frequency increases, the plot appears to be smoother, while at the low end of the spectrum the plot is more ragged. As a consequence of the averaging process, the lower frequency data will in general, appear noisier. In addition, peaks or resonances which may have appeared at the higher frequencies are attenuated by the averaging process. To discern these peaks a "search" of the original 8193 data is performed and the peak value occurring within each averaging interval is extracted, printed and plotted. For slowly varying PSD, the uncertainty of the "condensed" data can be shown to be proportional to $\frac{1}{\sqrt{N}}$ within each averaging interval, where N refers to the number of points averaged within an interval.

Much care should be taken in interpreting the plotted or printed results. Strictly speaking, in order for plots of PSD to be correct, they should be presented as bar graphs. This is true because each point represents a power level within a frequency range - $arcsec^2/Hz$. In attempting to extract rms values, the exact frequency increment must be known.

4.2.3 Verifying the Computer Reduction Process

The ability of the computer program to extract PSD was tested in both frequency and magnitude. Two different inputs were used to independently check these two areas. A 10 Hz square wave was recorded on the tape recorder and underwent the entire data reduction process. The results are shown in Fig. 4.5. This plot shows some even harmonics present where they shouldn't be and also some subharmonic content. A review of the raw data to the program indicated that because the counter averages the time for 80 pulses, the transitions in data are not as sharp as in an ideal square wave. The subharmonic content is a consequence of

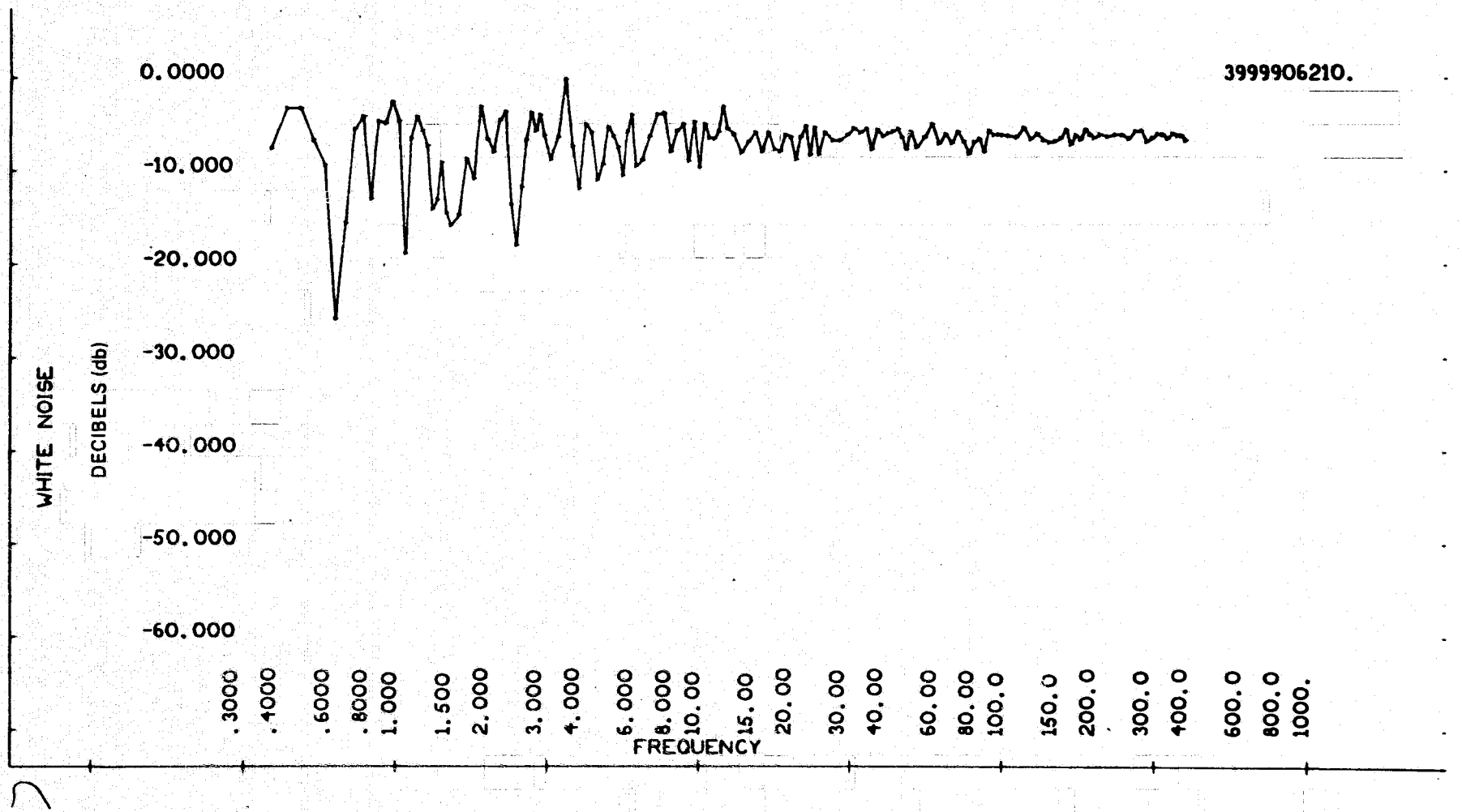

Fig. 4.4 PSD of Computer Generated White Noise High Frequency.

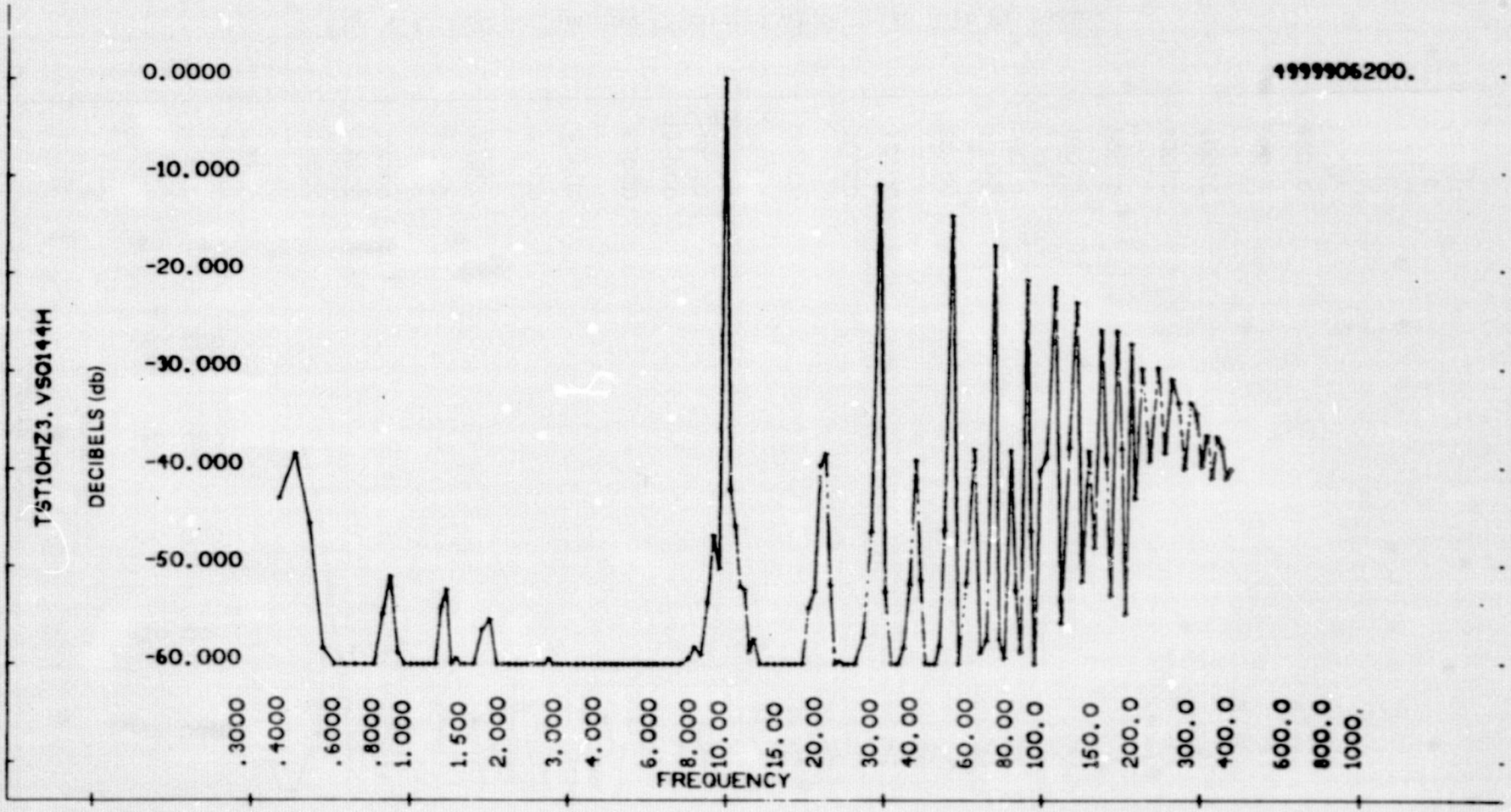

Fig. 4.5 PSD of 10 Hz Square Wave with "HOLD" in Program.

the same effect, not unlike the manner in which a sampling oscilloscope works. These observations were confirmed by performing the spectral analysis of ideal square wave data generated by a computer. The plot shown in Fig. 4.6 was generated and indeed does not contain the even harmonics or subharmonics. Thus, it is concluded that the frequency dimension of the spectrum analysis is correct.

To verify that the magnitude extracted was correct, band-limited white noise with a known standard deviation was computer-generated and analyzed. Figures 4.4 and 4.7 show the high and low frequency plots produced. Note in Fig. 4.7 that the digital filter begins attenuating near 25 Hz. Because it is known that the area under a power spectral density curve is equal to the mean square value of the random process, it was a simple matter of inspection to verify that the computed PSD area for white noise equalled the known mean-square value of the computer-generated noise.

4.2 4 Filtering and Bandwidth

The bandwidth and filter characteristics of the various items and operations in the test and data procedures are shown in Fig. 4.8. To preclude aliasing of higher frequencies (> 200 Hz) into the original data, the demodulator filter frequency was set at 200 Hz. Subsequent operations tend to further attenuate high frequency components.

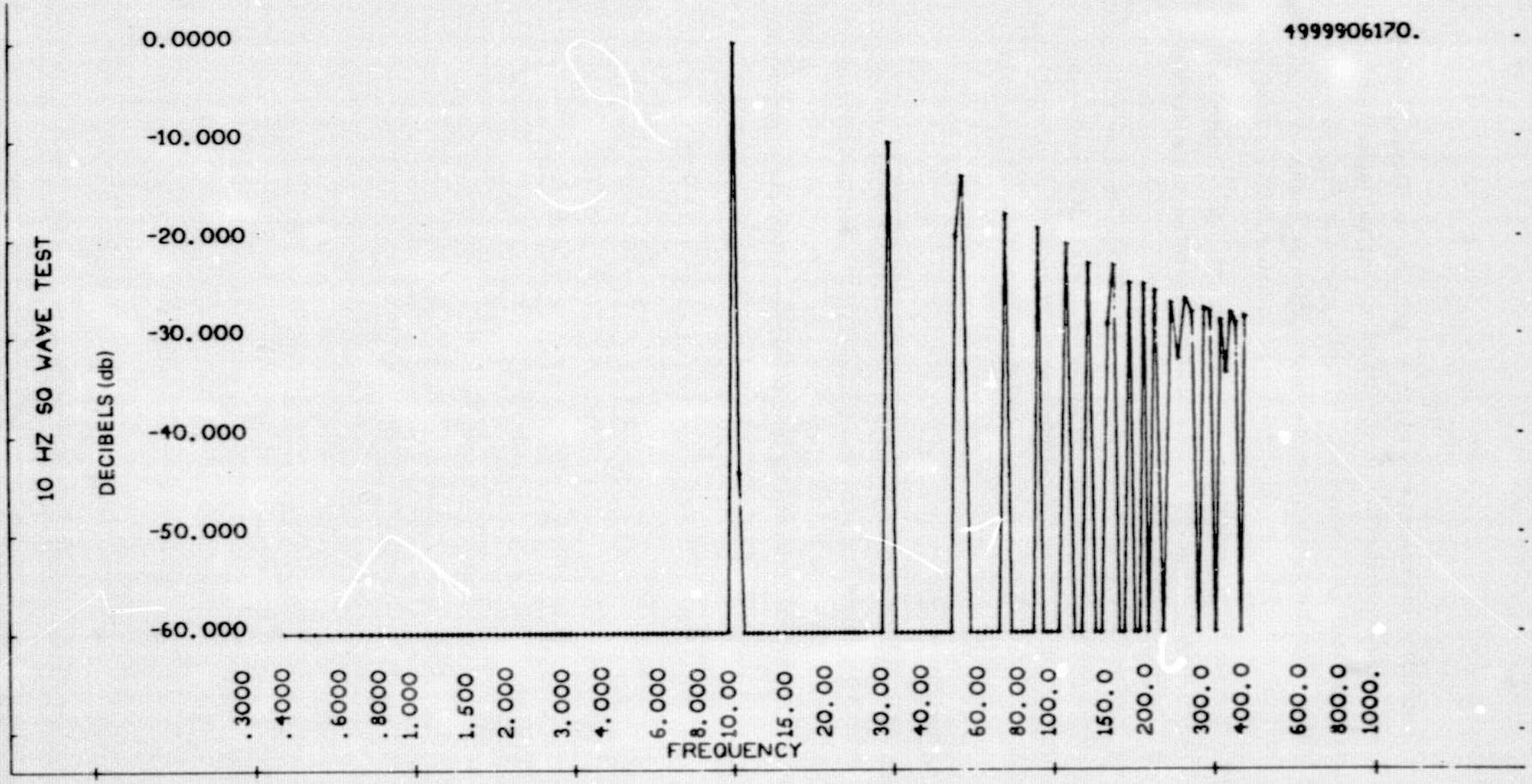

Fig. 4.6 PSD of Computer Generated 10 Hz Square Wave.

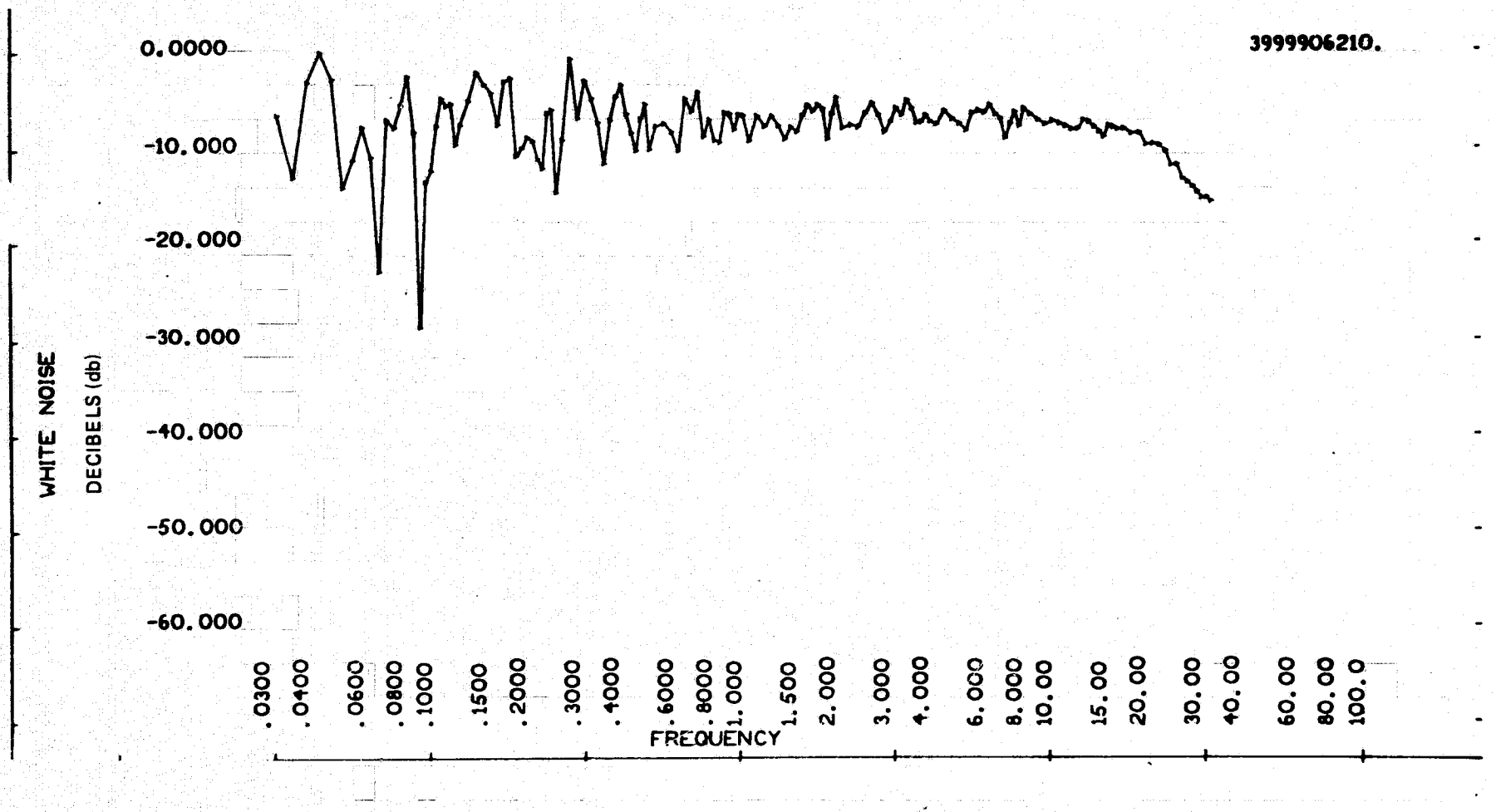

Fig. 4.7 PSD of Computer Generated White Noise Low Frequency.

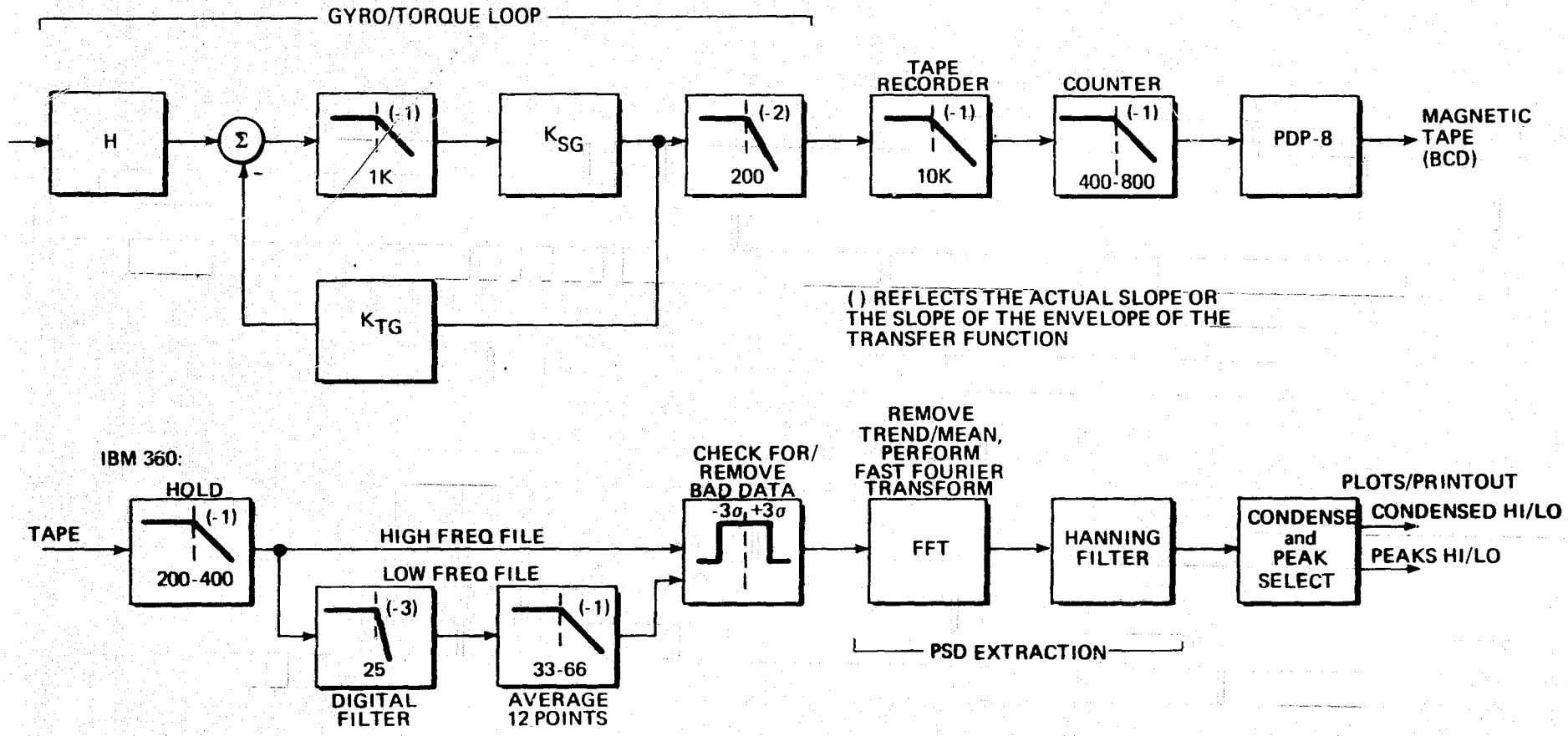

Fig. 4.8 Bandwidth and Filter Characteristics of Test and Data Reduction Steps.
(Breakpoint frequencies are in Hertz)

SECTION 5

INSTRUMENT TEST RESULTS

This section presents the results of tests performed on the following instruments:

MIT/CSDL TGG Viscous Integrator	
MIT/CSDL TGG 50 Series Pre-prototype	
MIT/CSDL TGG 50 Series Prototype	
MIT/CSDL 2FBG-6F OAO	
MIT/CSDL 25 IRIG	
MIT/CSDL 18 IRIG	
Nortronics	GIT-1B
Nortronics	GI-K7G
Honeywell	GG 334

Where possible, a consistent data package is presented for each instrument. This package includes a description of the instrument, unclassified performance characteristics available from the manufacturer and the PSD data accumulated in this test series. Where available these PSD data include results obtained with the output axis vertical, input axis vertical and with output axis vertical and wheel off.

To permit a comparison of the various instruments, PSD output plots have been linearized to show magnitudes, slopes and resonances. The linearized plots were obtained by fitting straight-line segments to the computer generated PSD plots with the constraint that the variance of the data was equal to the sum of the variances of the resonances plus the area under the linearized curve, i.e., the total power in the linearized plot is equal to the measured power. Because a certain amount of judgment was required to "linearize" the plots, the computer-generated PSD plots are included as the Supplement to this report.

The characteristics of all the instruments tested are shown in Table 5.1. Tests and results for each instrument are described in the following paragraphs.

CHARACTERISTIC	UNITS	GYRO								
		MIT/CSDL						NORTRONICS		HONEYWELL
		TGG VI	TGG PROTO	TGG PREPROTO	2FBG-6F-OAO	25 IRIG	18 IRIG	GIT-1B	K7	GG 334
WHEEL	TYPE	NO WHEEL	HEMISPHERICAL GAS		BALL	SPOOL GAS	SPOOL GAS	SPOOL GAS	SPOOL GAS	SPOOL GAS
H	gm-cm^2/sec		0.5×10^6	0.7×10^6	1.7×10^6	0.54×10^6	0.15×10^6	1.8×10^6	0.18×10^6	0.2×10^6
SPEED	RPM		32,000	24,000	12,000	24,000	24,000	24,000	72,000	24,000
RUN POWER	WATTS		16.5	~12	3	9	5	6	6.5	3.5
GAIN H/C		NA	1.2	0.87	1.9	0.5	0.2	1	9	0.4
CHARACTERISTIC TIME $(I/C)_{OA}$	MILLISEC	0.57	0.75	0.75	1	0.59	0.33	~1.0	4	0.5
TORQUE GENERATOR	TYPE	EM (2 winding)	EM (2 winding)	EM (2 winding)	EM (2 winding)	EM	PM	PM	PM	PM
SENSITIVITY	MERU	2.4/ma^2	5.2/ma^2	2.4/ma^2	0.165/ma^2	6/ma^2	120 eru/ma	*	7×10^3/ma	8×10^4/ma
MAX RATE		<100 eru	100 eru	<100 eru	40 eru	360 eru	60°/sec	*	3°/sec	110°/sec
SIGNAL GENERATOR	TYPE	EM E	EM BRIDGE	EM E	EM	EM	EM	EM	EM	EM
SENSITIVITY	$MV/MRAD_{OA}$	84	110 TUNED	84	34	32	20	~20	40	24
SUSPENSION	TYPE	EM TAPERED	EM TAPERED	EM TAPERED	EM TAPERED	EM TAPERED	EM TAPERED	EM	TAUT WIRE	DITHER JEWEL
RADIAL TC		8 min	8 min	8 min	*	*	*	*	*	*
AXIAL TC		3.4 hrs	3.4 hrs	3.4 hrs	*	*	*	*	*	*
OPERATING TEMP.	°F	121	135	135	135	135	132	180	170	180
MOUNTING CONFIG.		END STUD	TAPERED END STUD	END STUD	END STUD	END STUD	END MOUNTED	END STUD	CENTER FLANGE	CENTER FLANGE
ENVIRONMENT		NA	MISSILE BOOST	MISSILE BOOST	SATELLITE	MISSILE	SATELLITE	GYRO COMPASSING	NAVIGATOR SATELLITE	30g max
LIFE EXPECTANCY	MTBF (hrs)	NA	100K	100K	20K	*	*	*	100K	NA

*NOT AVAILABLE

Table 5.1 Summary of Instrument Characteristics.

5.1 MIT/TGG Viscous Integrator (SN 293)

This instrument is a Viscous Integrator (VI) (no wheel) version of the pre-prototype 50 series Third Generation Gyro (TGG). It uses electromagnetic ducosyns and was constructed with a 93 dyne-cm unbalance along -SA. PSD tests were originally performed to evaluate test and data taking techniques without tying up a gyro. However, as it turned out, much of its data helped with the interpretation of TGG gyro data.

5.1.1 Test Results — VI 293

The tests were conducted at the MIT/CSDL Inertial Gyro Group Test Laboratory. The instrument was mounted on a D-table which is bolted to the floor of the building. Because the VI contains no wheel to provide earth rate coupling, the signal generator was calibrated against gravity with a prior knowledge of unbalance (dyne-cm) and damping (dyne-cm/rad/sec). The linearized PSD results are shown below. The plots in addition to several resonances, shows a minus one (- 10db/ decade) slope in power. The resonances in the bandpass between 25 and 100 Hz are attributed to the environment, since many of the frequencies noted have been confirmed on other occasions by the Inertial Gyro Group.

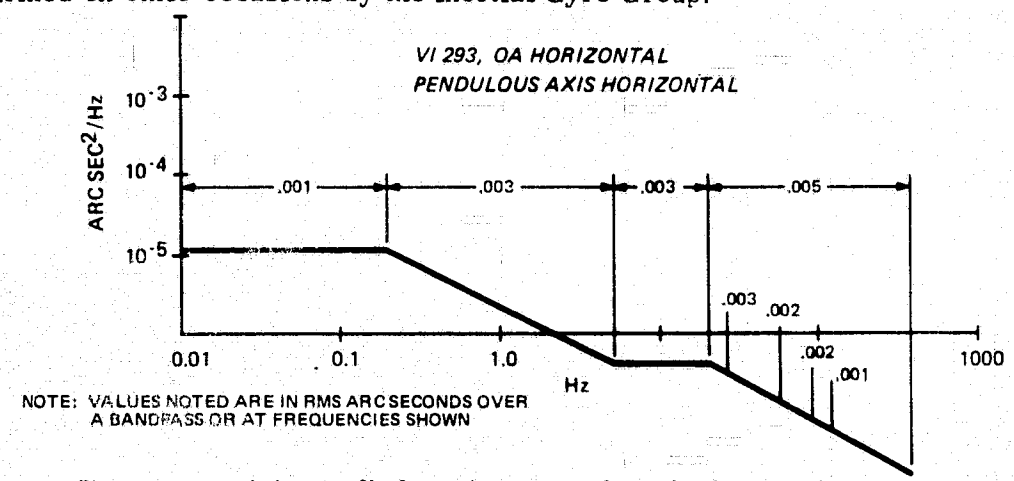

It was surprising to find a minus one slope in the data because slopes in power for linear, lumped systems occur in integer powers of two. The data taking and processing steps were reviewed in search of a possible cause of the minus one slope. Finally, it was concluded that this slope was a legitimate characteristic of the instrument's output caused by internal noise (mechanical or electrical), support electronics or base motion.

A mechanism exists in semiconductor electronics which is characterized by a minus one slope. It is referred to as "flicker" or "1/f" noise and results from the random process in charge carrier motion on the surfaces of semiconductor materials. Although it was not possible to examine how "1/f" noise in the various

excitation sources supporting the instruments could affect the results, a test was conducted to determine the PSD of the SG amplifiers and recording equipment noise. A 50 Series SG microsyn secondary was used as a source at the input and the signal gain was set to a nominal value of 30,000 — 50,000 was the highest gain used in the test program. The results displayed a white noise characteristic, i.e., a flat PSD. The standard deviation was 0.004 mv in the passband from 0.03 Hz to 300 Hz. This indicates that in the frequency range of interest 1/f noise from these sources does not predominate.

The amount of base motion required to introduce the recorded VI PSD was analyzed. Normally, float-to-case motion for the VI is introduced in two ways: 1) angular rate about the OA is coupled through the float's inertia and 2) linear accelerations are coupled through the mass unbalance. The equation describing VI dynamics is:

$$I(\ddot{A}_{I-C} + \ddot{A}_{C-F}) + C\dot{A}_{C-F} + RA_{C-F} = m\ell a - KA_{C-F}, \text{ in which:}$$

A_{C-F}	=	Float-to-case angle	
A_{I-C}	=	Case angle relative to inertial space	
I	=	Float inertia about OA	306 gm-cm^2
C	=	Float output axis damping coefficient	8.5×10^5 dyne-cm/rad/sec
$m\ell$	=	Mass unbalance (per g)	93 dyne-cm
R	=	Restraint torque coefficient	Negligible
K	=	Torque loop constant	
a	=	Linear acceleration (in g's)	

Laplace transforming the equation and arranging the results in transfer function form float-to-case angular motion is described by:

$$A_{CF}(s) = \frac{\frac{m\ell}{K} a(s)}{(\tau_L s + 1)(\tau_F s + 1)} - \frac{I/K\, A_{I-C}(s)}{(\tau_L s + 1)(\tau_F s + 1)}$$

where:

$$\tau_L \simeq \frac{C}{K}$$

$$\tau_F \simeq \frac{I}{C}$$

With a feedback loop such that a 40-second time constant, (τ_L) is achieved, we have;

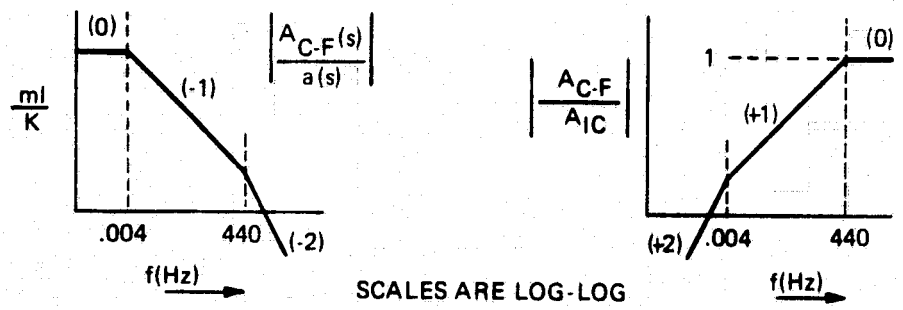

Since it is not possible to separate the two inputs, the effects of angular motion about OA and linear acceleration were treated individually. That is, the PSD in angular motion alone was computed to produce the observed PSD of the VI output. Similar calculations were performed for linear acceleration assumed to be acting alone on the VI. The computed rms value of inputs that would be required to give the observed case to float motion in the frequency range 0.004-30 Hz are:

$$\measuredangle \text{ rms} = 320 \text{ arcsec}$$

$$\mu g \text{ rms} = 7000\, \mu g$$

Obviously, this amount of base motion is unreasonable, and is therefore discounted as the source of the minus one slope.

5.2 MIT Third Generation Gyro-Prototype

The TGG is a medium-size gyro originally designed to NASA's high performance and reliability requirements and later modified for use on Air Force programs. The stated goal for random drift steady-state operation is 0.001 meru for a 30-day period. It incorporates hemispherical gas-bearings and electromagnetic ducosyns.

5.2.1 Tests and Results TGG Prototype

Two TGG prototype gyros were tested at the Inertial Gyro Group Test Laboratory in Cambridge, Mass. SN 212 was tested early in the program but because the wheel-off data were "lost" during the computer reduction process, SN 213 was tested to provide data for the TGG wheel-off characteristics. The seismic environment in which 213 was tested, however, was extremely "noisy" — so much so that vibration from pumps and other equipment could be felt. The effect of this noise is shown in the wheel-on data obtained from this instrument which is exceptionally high but exhibits a minus two slope at higher frequency. The linearized plots of PSD for the two instruments are shown in Fig. 5.2.1.

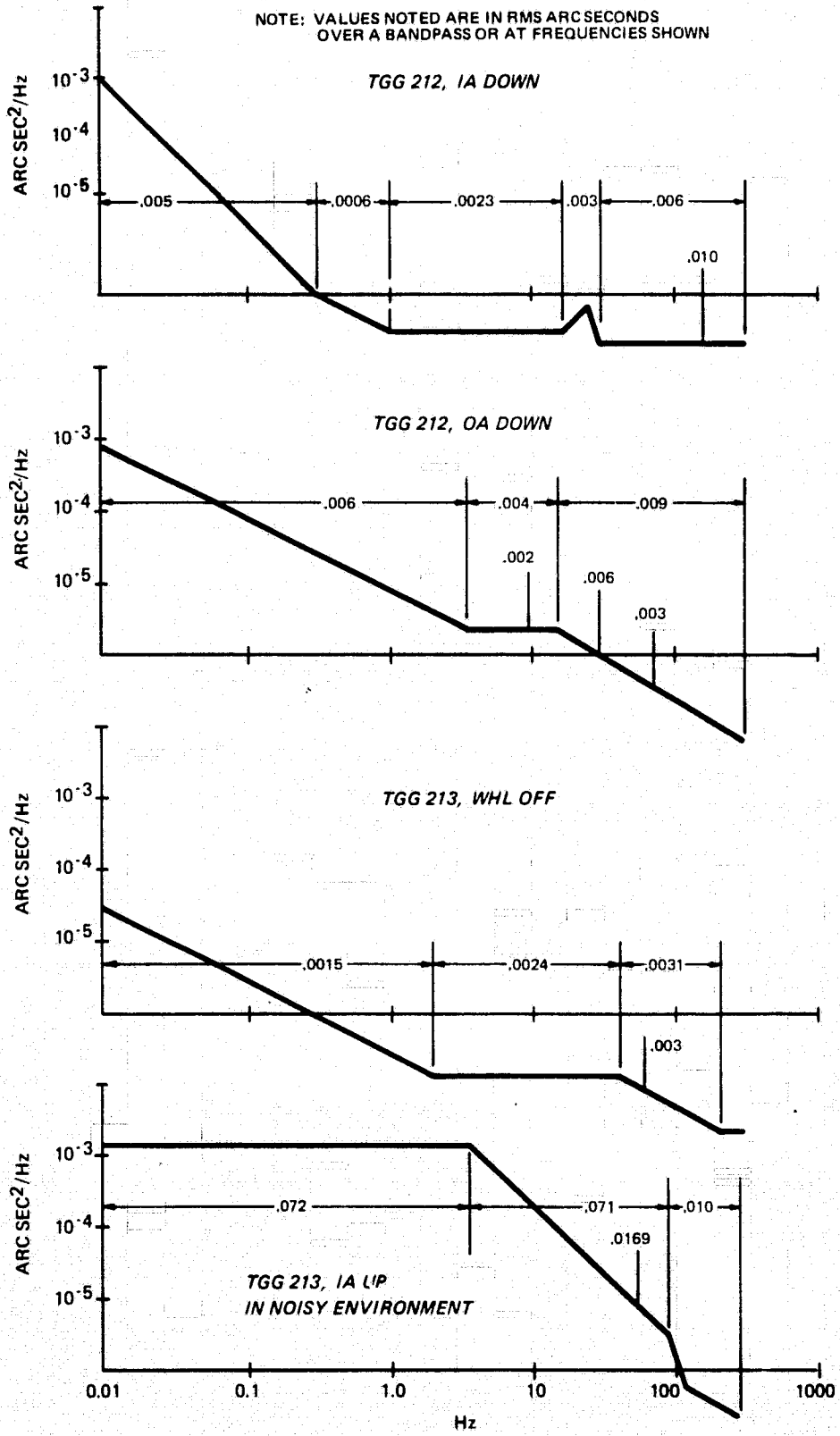

Fig. 5.2.1 Linearized PSD Results from Two TGG Prototype Gyros.

The wheel-off data (Fig. 5.2.1) exhibits characteristics similar to the VI version of the TGG discussed in Section 5.1, that is, the noise level at frequencies above 2 Hz is low (1.5×10^{-7} arcsec^2/Hz) with a minus one slope through the lower frequencies. The wheel-on data from SN 212 also exhibits a minus one slope. Since both wheel-off and on data exhibit the minus one slope it is concluded that this characteristic is probably a function of either instrument magnetics, the float, fluid, case configuration or electronic support equipment rather than noise induced by wheel operation or base motion.

The TGG gyro exhibits the minus one slope to frequencies below 0.1 Hz. This will result in reduced error growth rate (compared with instruments which possess more negative slopes in this frequency range) as data is sampled for longer periods and is in keeping with the performance goal of this instrument which is is in the 0.001 meru (1.5×10^{-5} °/hr) region.

Finally, it is worth noting that the power supplies employed by the IGG group are all regulated to 50 ppm/wk and the nominal temperature controller gains are of the order of 10,000 watt/°F.

5.3 2FBG-6F-OAO

The 2FBG-6F was originally designed for missile guidance systems for the Air Force. Modifications for the OAO satellite application included reduced ball-bearing preload, tapered electromagnetic suspensions, and the elimination of balance hardware. It is a large gyro ($H = 1.7 \times 10^6$) which has exhibited random drift stabilities close to 0.05 meru over a 30-day period. The main reason for testing this gyro was to compare gas-bearing and ball-bearing gyros which exhibit comparable long-term performance. The 2FBG-6F-OAO was the only ball-bearing gyro tested.

5.3.1 Test Results -- 2FBG-6F-OAO

Only one set of data were accumulated on this instrument and these were with output axis vertical. The linearized PSD plot shown below indicates a region between 13 and 55 Hz in which the many discrete frequencies recorded result in a standard deviation of 0.102 arcsec.

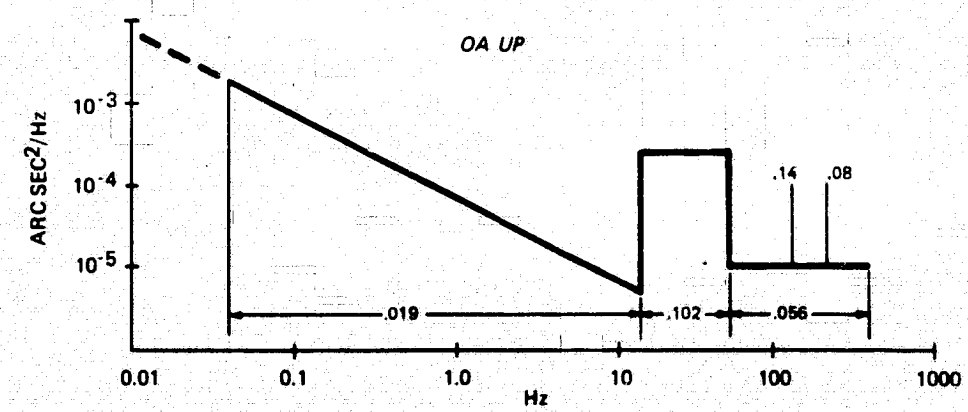

There appear to be no significant resonances below 10 Hz. This, in addition to a minus one slope throughout the lower frequency range, explains why the 2FBG-6F-OAO performance surpasses that of other gyros which may have less high frequency noise but steeper slopes at the lower frequencies.

Because the 2FBG-6F-OAO was designed with reduced pre-load for lower wheel power and longer life, unbalance coefficients were not expected to be very stable. For this reason, the IA vertical data exhibited random behavior in the arcsec region. Therefore, IA vertical data were not accumulated on magnetic tape. Wave analyzer plots with linear plots of drift are shown in Fig 5.3.1. In these data it is possible to compare wave analyzer plots and extract, if only qualitatively, resonances due to base motion. For example, resonances in the 10 Hz region which are evident in the OA vertical but not the IA vertical data may be attributed to base motion

5.4 MIT Third Generation Gyro -- 50 Series Pre-prototype

A pre-prototype version of the TGG gyro was tested at the Skipper Test Facility at Bedford. Except for some minor differences noted in Table 5.1, the pre-prototype is physically identical to the prototype.

5.4.1 Tests and Results -- TGG Pre-Prototype

In the test series performed on SN204, output axis vertical and two sets of input axis vertical data were accumulated. The two IA vertical data sets were separated by two days to determine whether or not the data represented a stationary process. The data in Fig. 5.4.1 marked "211" (Julian day) were recorded at 3:00 AM whereas the "213" data were recorded at 1:00 PM. This was done to identify any day/night variations in room temperature, cultural noise, etc. The two data sets show the random components to be within 2 db of each other and the overall standard deviations within 0.003 arcsec of each other. Thus, it is concluded that within the measurement passband, the process is repeatable.

The data accumulated on gyro 204 are somewhat noisier than the data accumulated on the prototype version. In particular, the minus two slope which causes the rms uncertainty to increase more rapidly with time. Since data accumulated on 204 and 212 by the IGG group indicates comparable performance, some other cause may be responsible for the difference in PSD.

A possible candidate is support electronics. It has been noted that although the Bedford Test Facility is seismically quieter than the Cambridge area, the electronic support equipment at IGG is superior with all excitations stable to 50 ppm/wk. The question of support electronics might just as well arise in terms of the other instruments tested. Perhaps a subsequent test series will investigate various instruments on the same test station resulting in common electronic noise and base motion inputs.

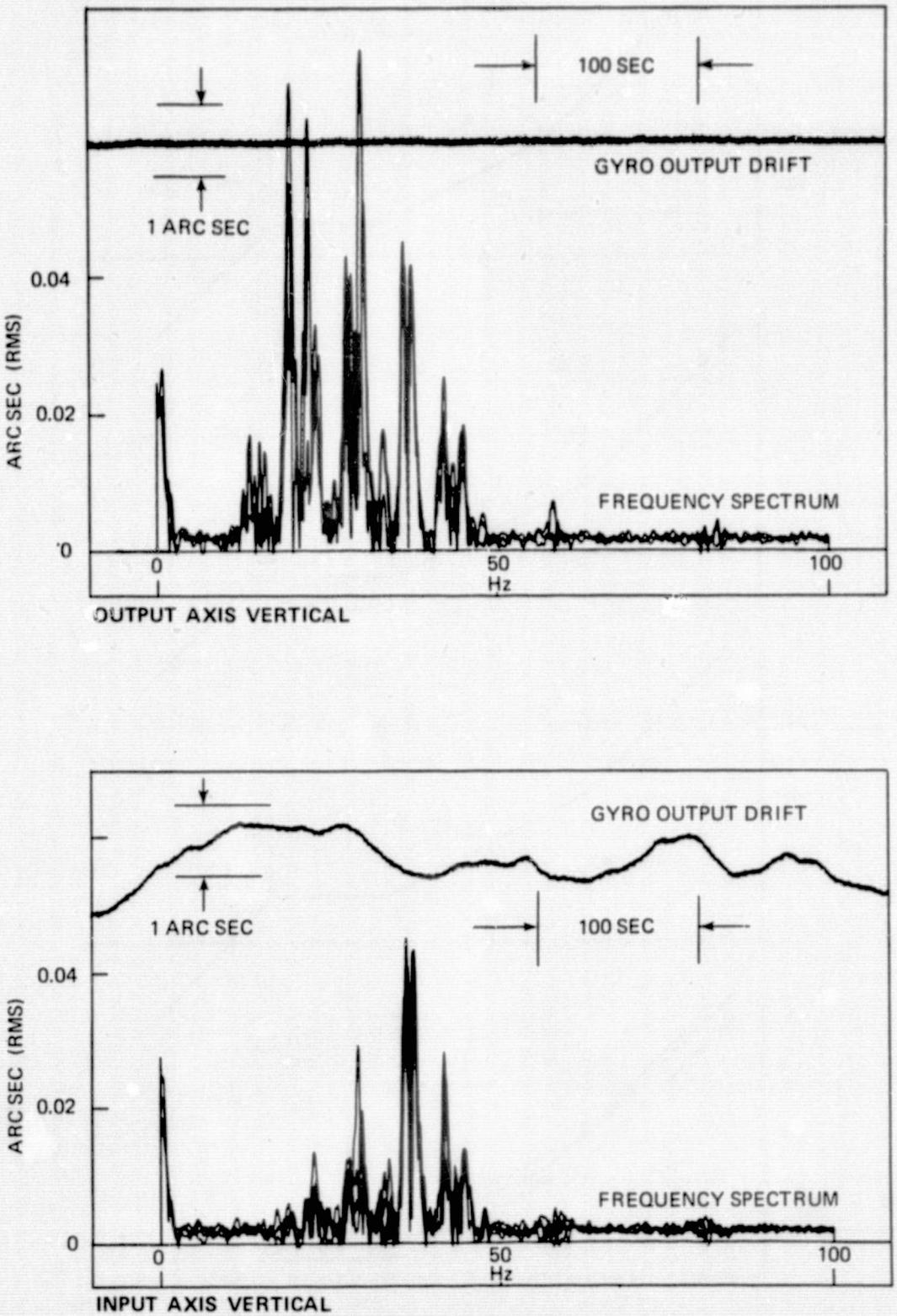

Fig. 5.3.1 Comparison of Drift and Spectral Characteristics for the 2 FBG-6F-OAO with OA and IA Vertical.

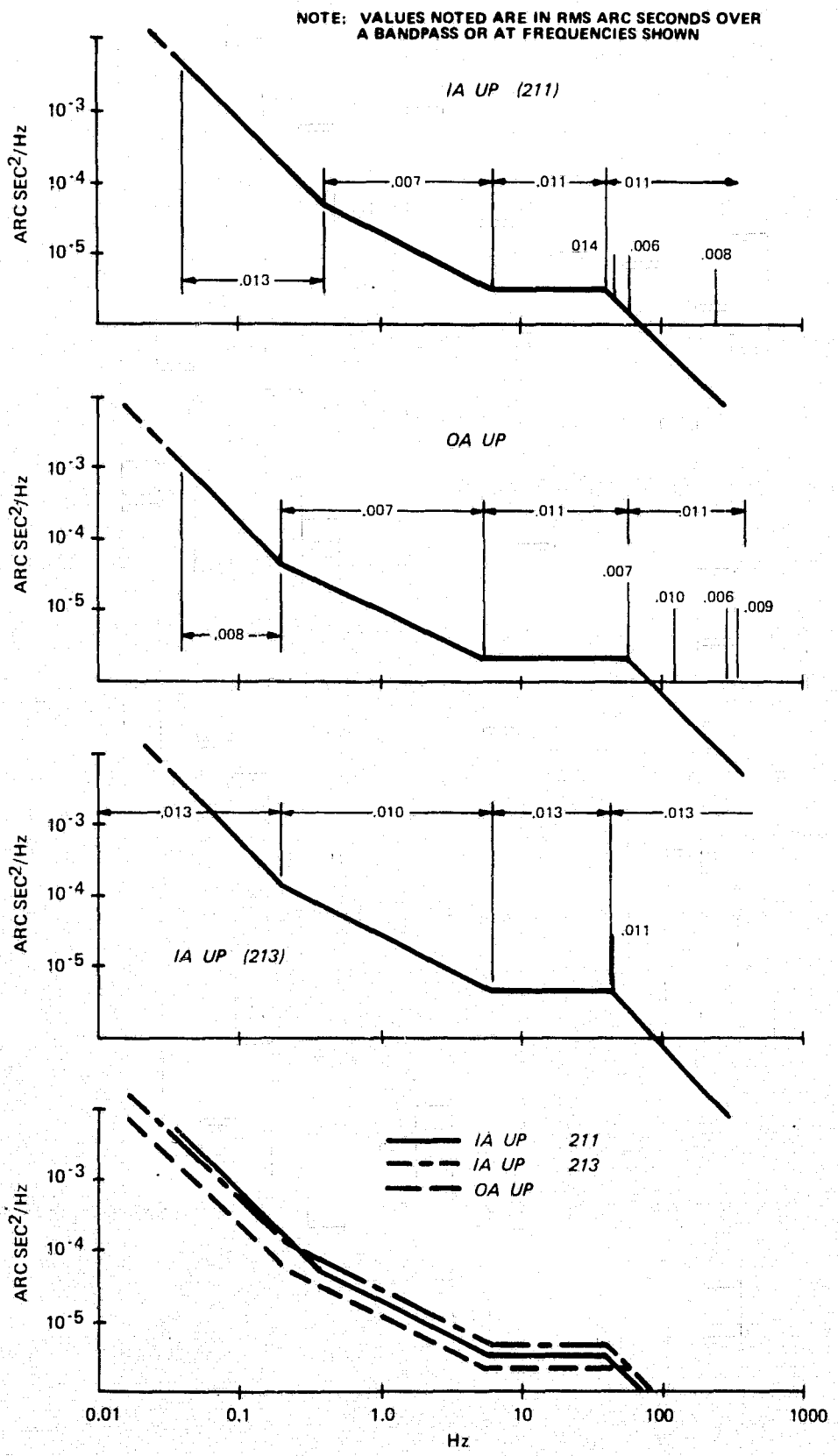

Fig. 5.4.1 Linearized PSD Results - TGG 204.

5.5 25 IRIG Mod 3

This gyro was designed by the MIT/CSDL Fleet Ballistic Missile (FBM) group for use on various navy projects. It features a spool gas-bearing ($H = 0.54 \times 10^6$) and electromagnetic ducosyns.

5.5.1 Test Results – 25 IRIG Mod 3

The 25 IRIG Mod 3 was tested at the FBM Gyro Test Laboratory in Cambridge, Mass. The linearized PSD results are shown in Fig. 5.5.1. Although there are no major design differences between the 25 IRIG and the other magnetically suspended gyros, its wheel-off data are inconsistent: the PSD below 0.4 Hz is white. Because on the following night an 18 IRIG was tested (Section 5.6) on the same stand using the same support electronics, this characteristic can not be attributed to electronics or base motion, but to the actual design features of the instrument. It would be interesting to compare the 25 IRIG with perhaps the TGG VI in search of mechanisms which may account for the difference in characteristics.

5.6 18 IRIG Mod B

Designed for NASA studies of strap-down satellite applications, the 18 IRIG Mod B features a spool gas-bearing ($H = 0.15 \times 10^6$), moving coil permanent magnet torquer with 60°/sec torquing capability and tapered electromagnetic suspensions.

5.6.1 Test Results 18 IRIG Mod B

The 18 IRIG was tested on the same station as the 25 IRIG. It was mounted on the same table, used the same support electronics and was tested at the same time of night. Despite the similar environment, there is little similarity between the two sets of data as shown in Fig. 5.6.1. The linearized PSD data in Fig. 5.6.2 indicate a minus one slope below 2 Hz regardless of orientation or wheel mode. For the 18 IRIG, this slope is a definite characteristic of the instrument. Comparing the 25 IRIG and 18 IRIG designs may provide some insights into the minus one slope mechanism.

5.7 Nortronics GIT-1B

The gas-bearing (spool, $H = 1.8 \times 10^6$) GIT-1B is a production gyro designed exclusively to be used as a north-seeking reference. For this particular application, the maximum torquing capability of the PM torquer was minimized, as were float-centering time constants. Data are available which document the performance of this instrument.

5.7.1 Test Results

The GIT-1B was tested at the Nortronics facility at Norwood, Mass. The gyro was mounted on an acceptance test station which is used in determining the instrument's East-West averaging (gyro compassing) capability. Because this

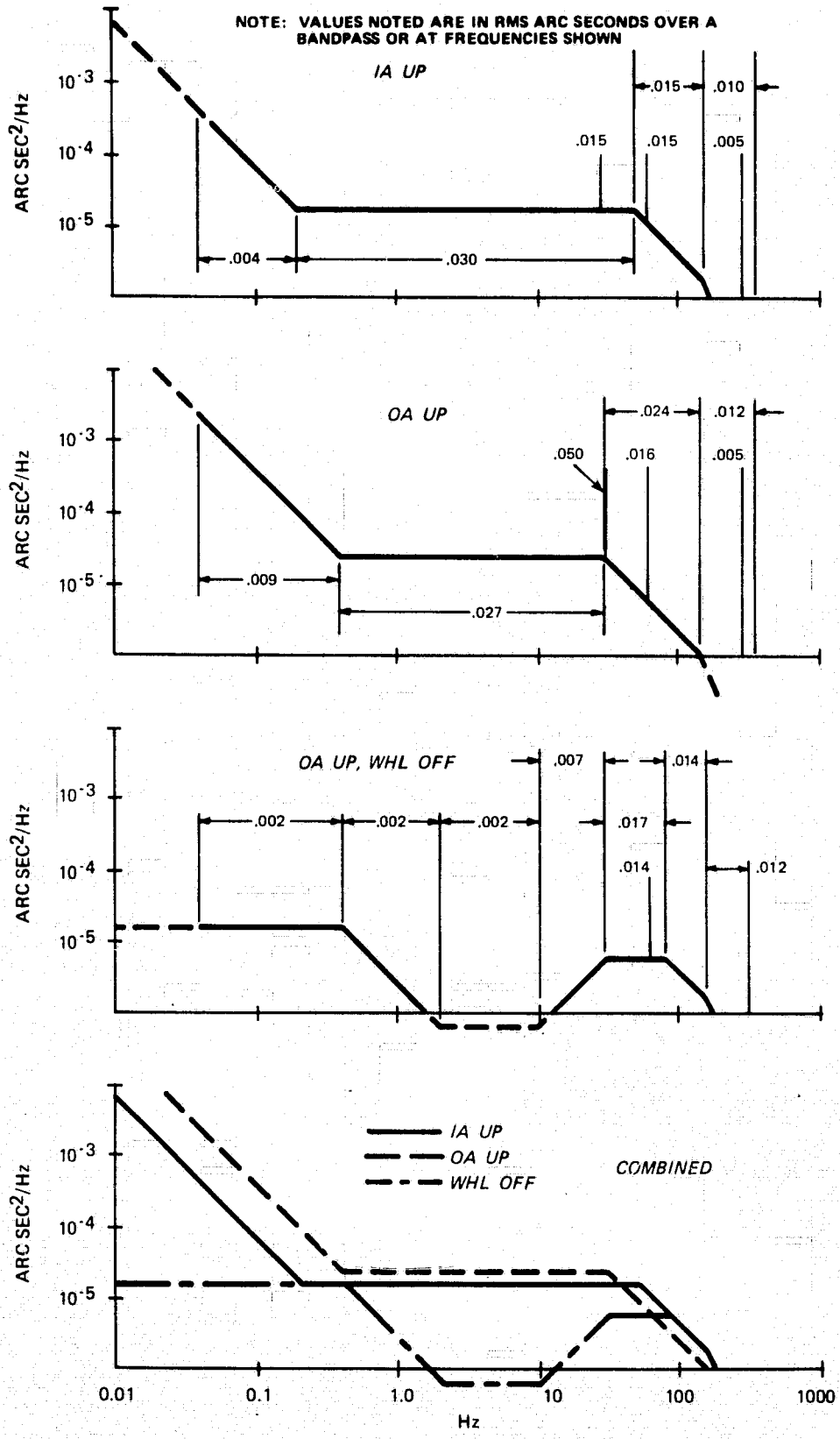

Fig. 5.5.1 Linearized PSD Results - 25 IRIG Mod 3.

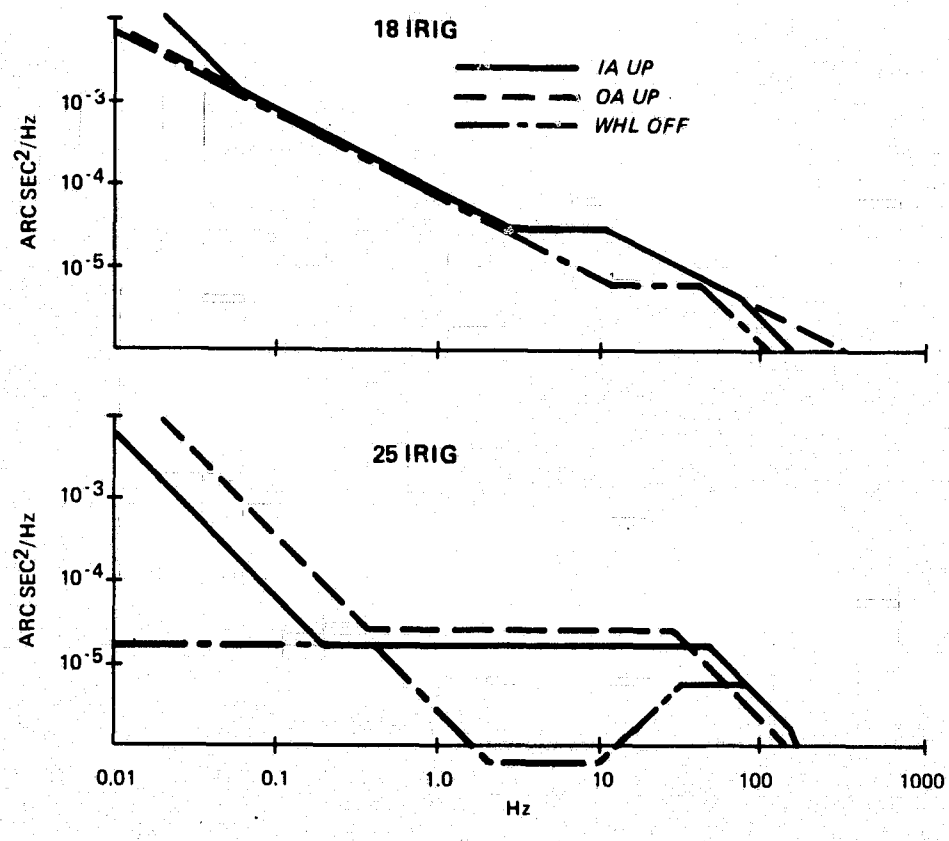

Fig. 5.6.1 Comparison of 18 IRIG and 25 IRIG Test Results.

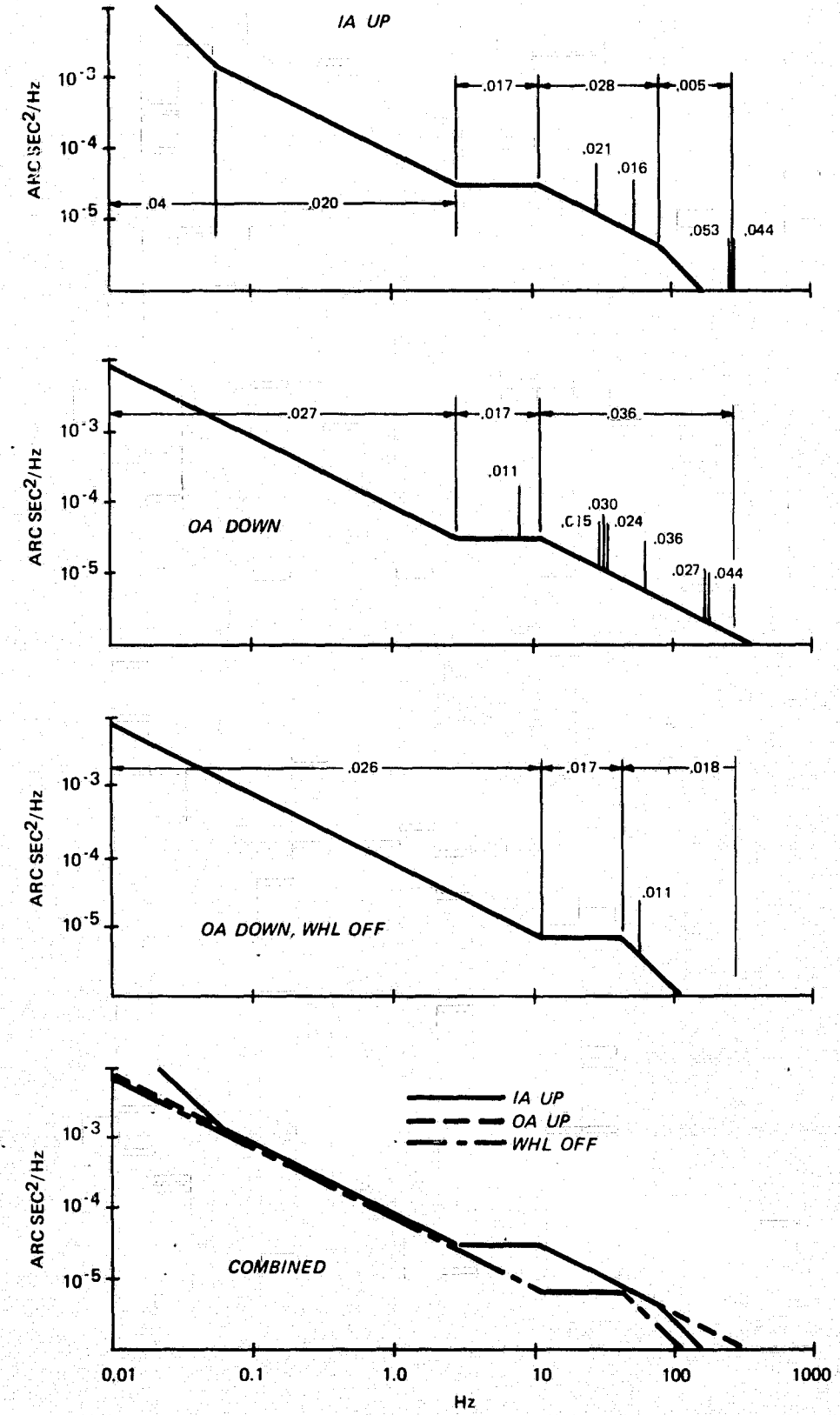

Fig. 5.6.2 Linearized PSD Results - 18 IRIG Mod B.

station is limited to rotations about a vertical axis the input axis up tests, were not performed. As a result, only output axis vertical and wheel-off data were accumulated. These data are shown in Fig. 5.7.1.

The wheel-on PSD exhibits the characteristics of white noise at frequencies below 4 Hz. The level is high, 10^{-4} arcsec^2/Hz; however, the zero slope below 0.1 Hz is consistent with the exceptional long-term performance exhibited by this class of instrument.

5.8 Nortronics GI-K7

A small (1.66" sq flange × 3.25" long) production gyro, the K7 is used in the C5 navigator and ESRO Satellite Guidance System. The gyro features a spool gas-bearing wheel (H = 0.18×10^6), permanent magnet torquer, paddle damping and taut wire gimbal centering. Much data are available from the manufacturer confirming wheel reliability (start / stop cycles) and torque repeatability from - 65°F cool downs.

5.8.1 Test Results - Nortronics K-7

The Nortronics K-7 gyro was tested at Norwood, Mass. During initial tests with a wave analyzer it was noted that instrument noise was up to an order of magnitude lower than instruments previously tested. The signal generator calibration procedure was repeated and the output sensitivity confirmed. The noise was indeed low as is illustrated by the linearized PSD plots in Fig. 5.8.1. Despite its low value at frequencies above 1 Hz, the wheel-on PSD below 1 Hz, increases with a minus two slope which results in uncertainties at 0.01 Hz comparable to some of the other instruments tested.

The only other gyro to indicate such a low level of noise at the higher frequencies is the GG 334. The two instruments have a common feature that sets them apart from the other instruments tested: they are not magnetically suspended. The K-7 float is maintained in place by an axial taut wire and the GG 334 applies a pivot and jewel arrangement, with a dithered jewel.

Does the taut wire method attenuate high frequency case to float motion by tying the float more closely to the case; or, do the magnetic suspensions introduce μ in. motion in the frequency range of interest? If radial motion is indeed present, then the SG null sensitivity to radial displacement (5-20 milliarcsec/μ in.) may be a possible mechanism. In any case, additional tests and analysis are required to determine whether the characteristics and dynamics of magnetic suspension systems are if only in part, responsible for the added high-frequency noise.

5.9 Honeywell GG 334

The Honeywell GG 334 is a gas-bearing gyro with an H of 2×10^5 and a

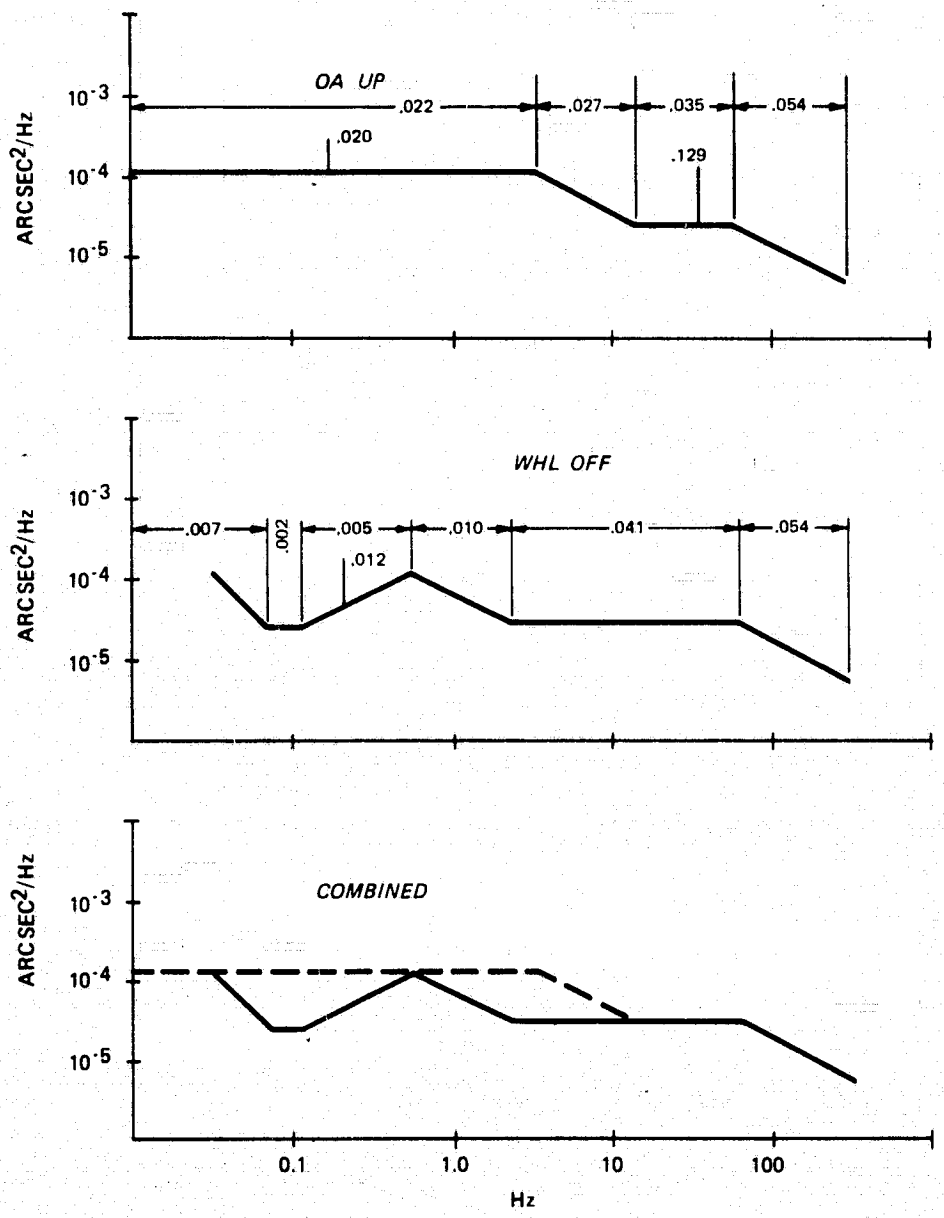

Fig. 5.7.1 Linearized PSD Results - GIT-1B

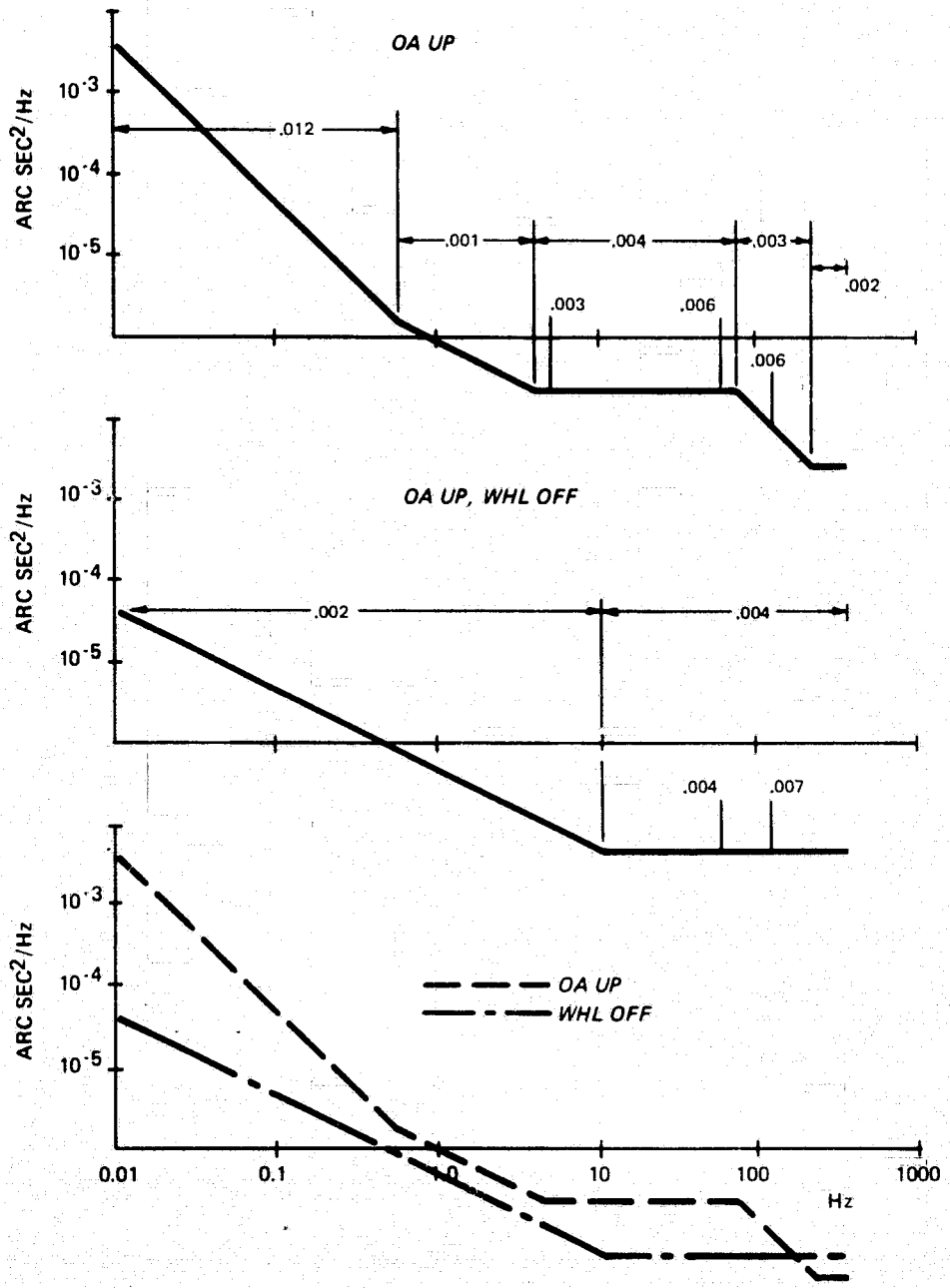

Fig. 5.8.1 Linearized PSD Results - GI-K7.

torquing capability of 2 rad/sec. It incorporates a dithered jewel-pivot output axis bearing.

5.9.1 Test Results GG 334

The tests on the GG 334 were conducted at the Honeywell Plant in Minneapolis, Minnesota. The instrument was mounted on a dividing head and the pier on which it was mounted rested on the floor of the laboratory which is a 5-foot thick slab of concrete approximately 30' × 50'.

Initial wave analyzer recordings of rms noise were much lower than other instruments tested. Following these observations, the value of the recording sensitivity was confirmed and some tests were performed to establish whether the float was "hung up". Figure 5.9.1 shows the output response to 0.1 arcsec step inputs: The float appears to return smoothly. The reduced level of noise is evident in the linearized plots of PSD shown in Fig. 5.9.2. For frequencies above 1 Hz the power content is one to two orders of magnitude below the power levels observed in the other gyros tested in this program. Why? Again the suspension system may be at least partially responsible. At one point, during some preliminary testing, the station power was shut down. With the input axis vertical, output noise was noted, after turn-on, as the instrument approached flotation temperature. The output noise increased as the instrument apparently passed perfect flotation. This observation indicates that although the dithered jewel is effective in reducing friction, the amount of friction will vary with temperature. The effectiveness of the dither is demonstrated by the fact that with wheel and dither off (wheel excitation drives the dither) the PSD is a factor of 10 greater than with wheel on at frequencies below 1 Hz.

Another possible explanation may be found in a Honeywell report by G. Kraus (Ref 6). This report describes a test series in which noise, in torque units, was recorded on a GG 334 before and after a shroud was placed around the spin motor. It was shown that the shroud converted the air flow relative to the wheel from turbulent flow to laminar flow. This resulted in a sizable reduction in output axis noise. Plots of gyro noise published in Kraus's report are shown in Fig. 5.9.3.

It is difficult to quantitatively compare the Honeywell data with the MIT data, because the two use different units (torque vs angle) and presentation (linear vs log-log). Qualitatively, many characteristics compare favorably. In particular, the peaks appear at the same frequencies and the relative noise between wheel off and wheel on at the lower frequencies is consistent.

What is most interesting about the data in Fig. 5.9.3, however, is that the amplitude of the no-shroud data is up to two orders of magnitude greater than the shroud data and that almost two orders of magnitude separates the GG 334 from most of the other instruments tested.

It is not implied that if the other instruments had shrouds their output noise would be improved more than a factor of 10. It is however, suggested that the necessary analysis be performed to evaluate whether turbulence torques are a possible cause of high-frequency noise in the various other instruments.

Finally, the PSD increases rapidly at frequencies below 1 Hz. This characteristic is consistant with long-term data accumulated on the GG 334 which is in the 0.1* to 0.3 meru (random drift) region.

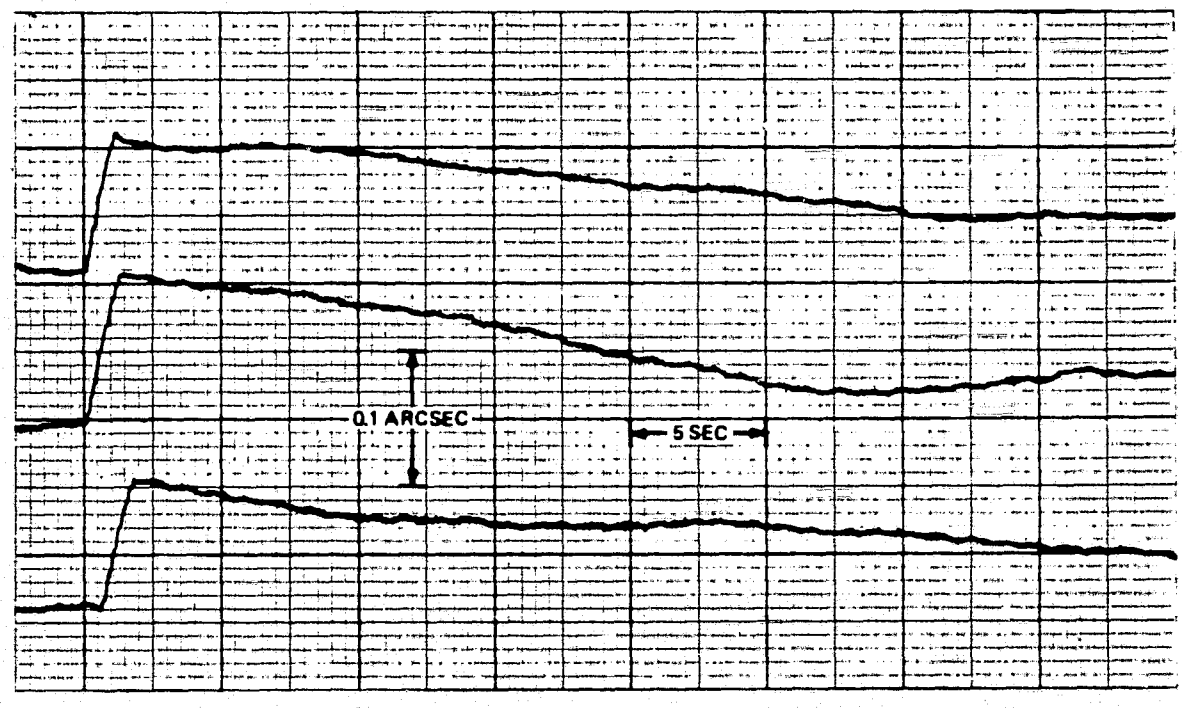

Fig. 5.9.1 GG 334 Float Response to 0.1 arc sec Step Inputs.

* System data supplied by Honeywell exhibits standard deviations of 0.1 meru (1σ) for 2-minute samples across 16 hours.

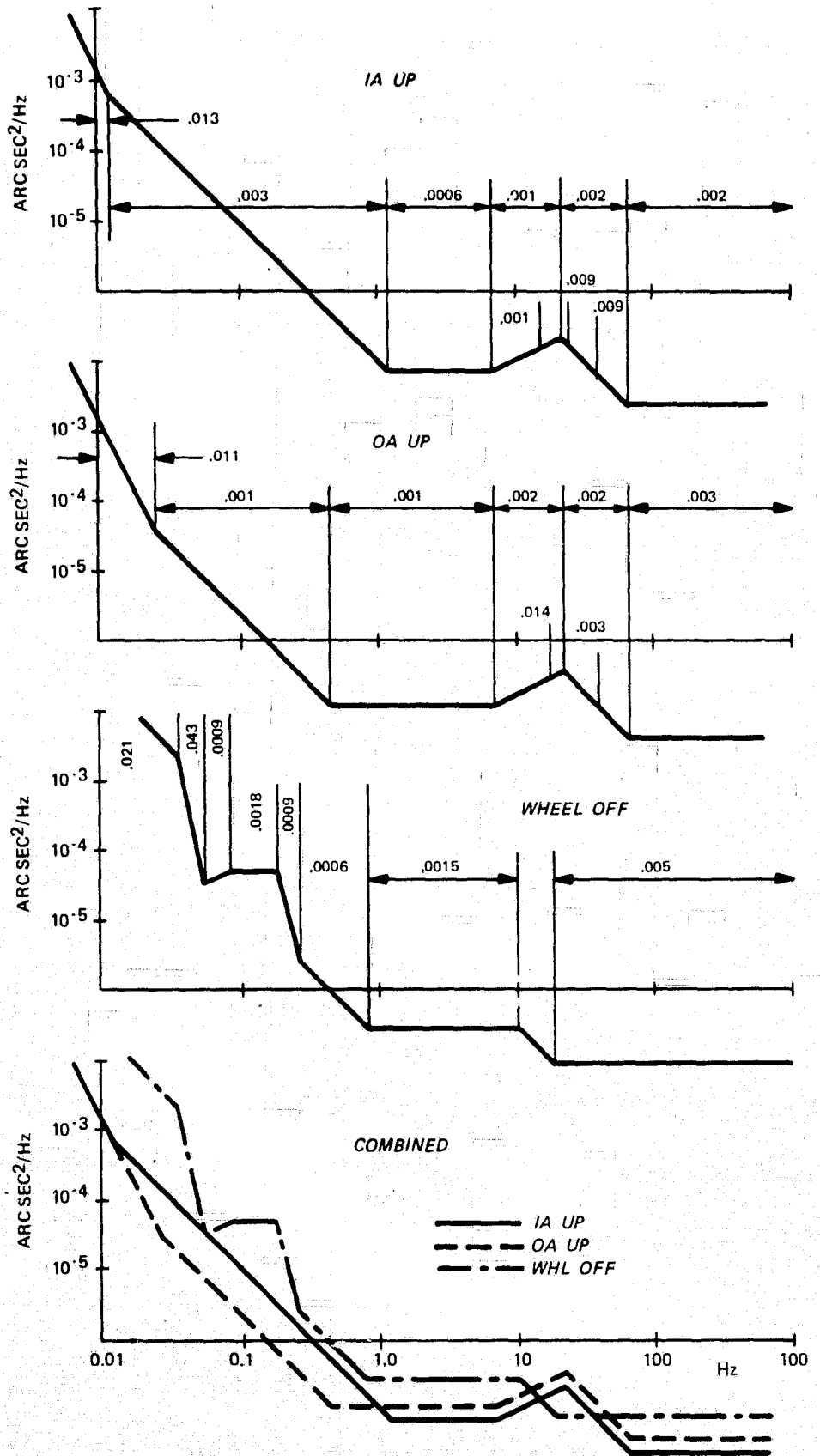

Fig. 5.9.2 Linearized PSD Results - GG334.

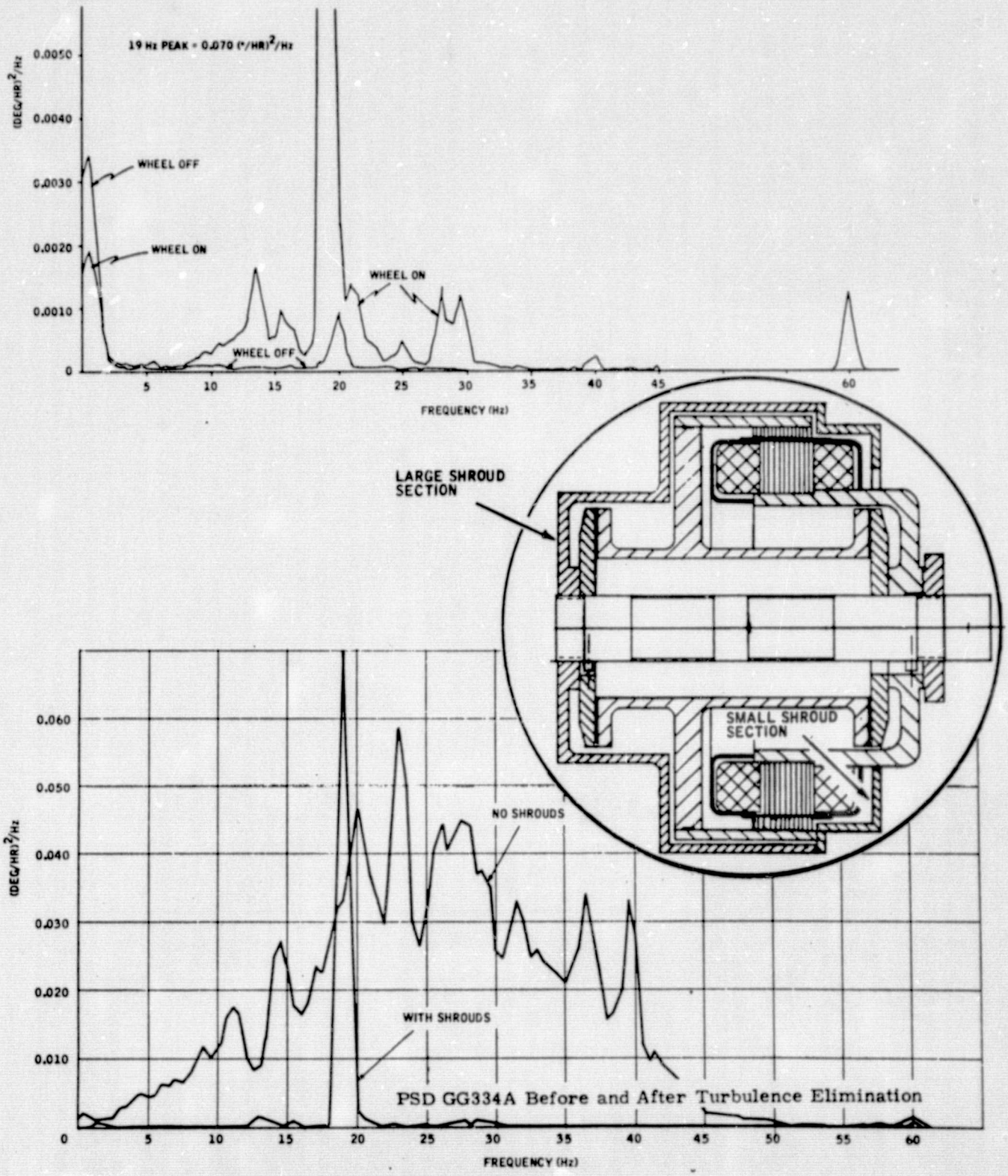

Fig. 5.9.3 GG 334 Data from Honeywell Report Showing Noise with and without Motor Shroud.

SECTION 6

THE MINUS ONE SLOPE IN SPECTRAL DENSITY

If one assumes that (1) the gyroscope and associated feedback circuitry can be modelled as a linear time-invariant system and that (2) for the frequency range of interest, noise can be represented by filtered white noise processes, it is straightforward to show that the measured spectral density presented on log-log paper will exhibit slopes that are even powers of two, e.g., -2, 0, 2, etc. This is a consequence of the fact that power transfer functions of linear systems with rational transfer functions can be asymptotically approximated by combinations of terms of the form $(a^2 + \omega^2)^{\pm n}$ for n = 0, 1, 2.... The spectral density plots characterizing several of the instruments described in this report possess minus one slopes over significant portions of the frequency range of interest. The purpose of this section is to discuss the presence of the minus one slope, speculate about its origin and point out that it is not peculiar to gyroscopic instruments.

6.1 Significance of Minus One Slope

The occurrence of a minus one slope in a power spectral density plot allows one to make several conclusions. First, for those zero mean random processes which have a finite mean-square value, the minus one slope cannot continue toward 0 or ∞ in frequency. This is shown by the following. The area under a PSD plot (from 0 to ∞ in frequency) is equal to the mean-square value of the process. The area under a PSD plot with a minus one slope that approaches 0 and/or ∞ in frequency is infinite. This contradiction indicates that the minus one slope can only exist exist over a finite range of frequencies. Incidentally, one can also show that a PSD which is flat heading toward zero frequency must exhibit a slope more negative than minus one at frequencies approaching ∞ in order that it characterize a process whose mean-square value is finite. It is worth noting, however, that some noise processes need not have a finite mean-square value. For example, the random walk process, generated by integrating white noise, does not possess a finite mean-square value. Clearly, then, if an angular rate noise process were white, the angle process would be that of random walk, and the variance of the process would approach infinity as time passed. One can conclude that gyro angle data need not possess finite mean-square value as time approaches infinity.

Second, the minus one slope over a range of frequencies may be described by the expression, "constant power per decade". This may be shown by integrating the $1/\omega$ spectral density over the frequency range a to b and observing that the result is proportional to $\ln\frac{b}{a}$, whose value only depends on the ratio b/a. Hence, the power contained over one decade of frequency is the same for every decade in which the minus one slope is present. Several examples of physical processes which are known to possess minus one slopes over portions of their PSDs are described in the next few paragraphs.

6.2 Examples of Random Processes whose PSD Exhibit Minus One Slope

The most common example of a random process whose PSD exhibits a minus one slope is found in the study of noise in electron tubes and semiconductors. These noise processes have been studied for several decades (Ref 1). The work has conclusively shown that these amplification devices inherently generate noise whose PSD contain a minus one slope over portions of the spectrum, primarily at low frequencies. This minus one slope has given rise to the term 1/f noise which is sometimes referred to as flicker noise.

Recent investigations with semiconductors (Ref 2) has established that for decreasing frequency the minus one slope breaks to zero slope at about 2×10^{-4} Hz. For increasing frequencies the minus one slope breaks to a more negative slope (specifically, minus two) at about 10^4 Hz. The mechanism which generates the 1/f noise involves the microscopic interactions of charge carriers, primarily on the surface of the electronic materials.

A second example in which a minus one slope in PSD has appeared occurs in wind velocity data (Ref 3). A common characteristic of wind and current flow in materials is that the processes can not be described by constant coefficient differential equations.

Both of the above examples may be considered as distributed parameter systems. It is suggested that such distributed parameter systems are potential sources of noise whose PSD contain minus one slopes. An example which serves to corroborate this conjecture occurs in the study of transmission lines. It can be shown (Ref 4) that the characteristic impedance of such lines can be expressed as an irrational function of frequency. For example, the impedance of one particular line is given by $Z = \sqrt{\frac{R}{Cs}}$ where R and C are distributed parameter constants describing the line. This expression is valid over a finite range of frequencies, not containing 0 or ∞. The irrational function of frequency is a direct consequence of the distributed nature of the transmission line. By contrast, transfer functions of lumped parameter systems are only expressible as rational functions of frequency, i.e., integral powers of frequency. It is suggested that in the presence of filtered

white noise, PSD measurements for systems containing transmission lines will exhibit minus one slopes. However, the authors are not aware of such data.

In Appendix B, it is shown how a distribution of the time constants in a group of first-order low pass filters can give rise to a minus one slope in PSD measurements.

6.3 Possible Sources of Observed Minus One Slope

It is possible that while 1/f noise in the electronics is present, it will not appear in the PSD of the instrument. This can happen if the other noise processes are of sufficient magnitude to "mask" the 1/f noise. Similarly, the 1/f noise may mask the other noise sources over a frequency range of interest. In this event, the PSD plot would not truly characterize noise processes within the instrument itself. Because a substantial amount of semiconductor readout electronics is employed in conjunction with monitoring the gyro output, 1/f noise may interfere with the measurement of the noise sources internal to the instrument. To date, tests have indicated that this is not the case for the frequency range of interest. As has been stated in a previous section, base motion is a possible source of noise whose spectral characteristics are inversely proportional to frequency over some frequency range. However, no definitive data on base motion has been found for the frequency range of interest.

Careful attention must be paid to identifying the sources of gyro noise. This is particularly important with respect to base motion. Although the results presented indicate that base motion is not a major noise source, one would like to test a gyro in a benign, motion-free environment. Otherwise, it would be difficult distinguishing noise produced by ground motion which the gyro would sense, from noise produced by internal gyro mechanisms. It is possible that the minus one slope is derived from ground motion, so instrument tests should be carried out to assess the significance of this and any other noise introduced by ground motion. In this way, value may be attached to the resultant PSD computations.

There may be still other mechanisms responsible for the minus one slope in PSD. For example, it is known that turbulence exists in the wheel-housing interface, generating noise power. Variations in wheel power can cause thermal gradients within the instrument. These variations may appear as undesired signal or noise. Also the magnetics in the torquer, signal generator, float suspension and wheel motor can generate noise due to microscopic motion of magnetic domains. This suggests the need for additional modelling of noise mechanisms within the gyro. The PSD presentations in this report may lend insight to reducing the effects of these noise mechanisms, and possibly identify others. Such work can only lead to a quieter and more precise sensor.

APPENDIX A

THERMAL NOISE CONSIDERATIONS IN SIGNAL GENERATOR DESIGN

It may be assumed that there are several mechanisms within a gyro that contribute noise to the measurement of signals of interest. In some gyro designs it is possible that a significant portion of the noise is developed in the signal generator of the instrument itself.

If it is found that the signal generator is a source of significant undesired noise over specific ranges of frequency several methods may be employed to reduce the effects of the noise. These methods are presented in this Appendix.

Part I Signal-to-Noise Power Ratio

In order to reduce the uncertainty of measurements, it is desirable to minimize the effects of noise sources within the gyro. As noise sources are identified, improved design methods may be employed to decrease their effect, while at the same time preserving the gyro's capability to measure signals of interest. This serves to maximize the signal-to-noise power ratio of the sensor. It is known that the signal generator in the gyro is a source of thermal noise, * a consequence of the random motion of charge carriers within the many turns of wire in the generator windings. This Appendix suggests several methods for increasing the signal-to-noise power ratio with respect to the thermal noise in the windings of the signal generator.

The problem is to determine the parameters of the network which couples the signal generator to the first stage of signal amplification (an operational amplifier) in a manner which maximizes the signal-to-noise power ratio. The structure of this network is largely fixed by electronic design considerations, e.g., appropriate tuning for quadrature rejection. The effect of the reactive portion of this network will be neglected in the following analysis for the reasons outlined below.

1. The reactive elements are needed to satisfy tuning requirements at frequencies higher than the useful bandwidth of the gyro. Hence, it is anticipated that they would not significantly affect low frequency operation.

---

*Thermal noise is characterized by a flat power spectral density over the frequency range $0 \leq f \leq 10^{13}$ Hz at room temperature.

2. Inclusion of the reactive elements would render the problem intractable and obscure the concept of maximization of signal-to-noise ratio.

By neglecting the reactive components, we may model the signal generator and coupling network as shown in Fig. A-1, where R_s represents the internal resistance of the signal generator, R_1 the op amp input resistor, and R_2 the input resistance of the operational amplifier itself. This model applies to an operational amplifier functioning in an unbalanced configuration. The signal which is amplified is denoted by e_o in Fig. A-1.

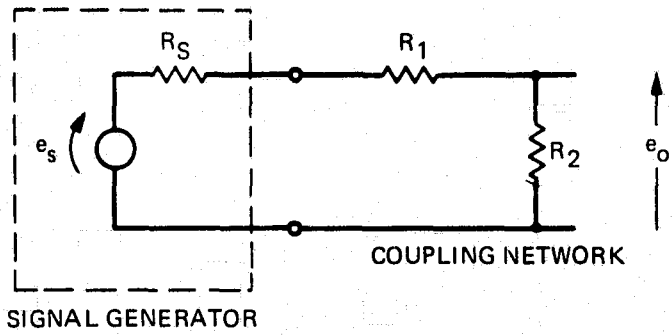

Fig. A-1 Circuit Model of Signal Generator and Coupling Network.

The entire network is assumed to be at the same temperature. To assume otherwise would needlessly complicate the calculations. That is, the results to be derived would be significantly in error only if temperatures (in degrees Kelvin) differed by a factor of 2 to 1. Generally, such temperature differences are less than $60^{\circ}F$, which justifies the assumption of equal temperature on the Kelvin scale. It is desired to find a relationship among R_s, R_1, and R_2 for which the signal-to-noise power ratio at the output, e_o, is maximized.

Define the following terms:

$$R_o = R_2 \,||\, (R_s + R_1) = \text{output impedance}$$

$$S_o = \frac{e_o^2}{4R_o} = \text{maximum output signal power}$$

$$S_s = \frac{e_s^2}{4R_s} = \text{maximum input signal power}$$

where the symbol || means "in parallel with" and for the example cited above is written mathematically as

$$R_o = \frac{R_2(R_s + R_1)}{R_2 + R_s + R_1} \tag{A-1}$$

Form the ratio S_o/S_s which is known as the available power gain, to which the symbol G is assigned. It is given by:

$$G = \left(\frac{e_o}{e_s}\right)^2 \left(\frac{R_s}{R_o}\right) \tag{A-2}$$

Also define the following terms:

N_s = input (source) noise power

N_o = output noise power

The relative noise figure of a system is commonly defined in terms of signal-to-noise ratios. We define it below:

$$\frac{S_o}{N_o} = \frac{1}{F}\frac{S_s}{N_s} \tag{A-3}$$

where F is the relative noise figure. Note that for $F > 1$ the output signal-to-noise ratio is less than the input signal-to-noise ratio. This always occurs in practice because the system (amplifier, network, etc) itself contributes noise to the output. For an ideal noise-free system, $F = 1$.

In order to maximize S_o/N_o, we will minimize F for the coupling network shown in Fig. A-1. Using the definition of available power gain we have:

$$S_o = GS_s \tag{A-4}$$

Dividing both sides by N_o, the equation below is obtained

$$\frac{S_o}{N_o} = G\frac{S_s}{N_o} \tag{A-5}$$

This expression for S_o/N_o may be set equal to that obtained in Eq (A-3) producing the result

$$F = \frac{N_o}{G\,N_s} \tag{A-6}$$

in which

$$N_o = G\,N_s + N_n \tag{A-7}$$

where N_n is the noise power introduced by the network itself. But for any resistive network, the available output noise power is given by

$$N_o = k\,T\,B_n \tag{A-8}$$

where

k = Boltzmann's constant (joules/^oK)

T = Temperature (^oK)

B_n = Measurement bandwidth (Hz)

Because the impedance of the signal generator is assumed resistive (see Fig. A-1), the available noise power associated with the signal generator itself is also given by $k\,T\,B_n$. Consequently we may write

$$N_o = N_s$$

Incorporating this information in Eq (A-6) we see that the relative noise figure F for the resistive network under consideration is given by*

$$F = \frac{1}{G} \tag{A-9}$$

for which a minimum value is sought.

An expression for F may be derived by substituting Eq (A-2) into Eq (A-9). The result may be put in terms of circuit parameters by employing resistive voltage division laws which relate e_o to e_s in Fig. A-1. Specifically,

$$\frac{e_o}{e_s} = \frac{R_2}{R_1 + R_2 + R_s} \tag{A-10}$$

*For a different development which yields this result for all resistive attenuators, see Ref 11.

The final result is

$$F = \frac{(R_s + R_1)(R_s + R_1 + R_2)}{R_2 R_s} \qquad \text{(A-11)}$$

For ease of presentation, let the following substitutions be made

$$x = R_s$$

$$a = R_1$$

$$b = R_2$$

The case of interest here is to minimize F with respect to x, holding a and b constant. This is a consequence of the fact that a and b are often fixed by amplifier design considerations, whereas flexibility in the choice of R_s is possible through the use of a coupling transformer or in the selection of the number of turns of wire in the signal generator. However, since there is some flexibility within certain constraints in the choice of a and b, minimization of F with respect to these variables will be considered as well. Recognize that the minimization is physically constrained by the conditions.

$$0 < x < \infty$$

$$0 < a < \infty$$

$$0 < b < \infty$$

since the use of negative resistors is not allowed.

The relative noise figure F is plotted in Fig. A-2 as a function of x, with a and b fixed positive constants. The necessary condition for a relative minimum to exist is $\frac{dF}{dx} = 0$ which is satisfied for

$$x_o = \pm \sqrt{a(a+b)} \qquad \text{(A-12)}$$

The minus sign reflects a physically unrealizable condition. The positive value of x_o is that value of x which minimizes F under the constraint $x > 0$. This is the condition we sought to find. It is a relationship among the network elements and source resistance which minimizes the relative noise figure. The corresponding minimum value of F may be computed directly using Eq (A-11) and (A-12).

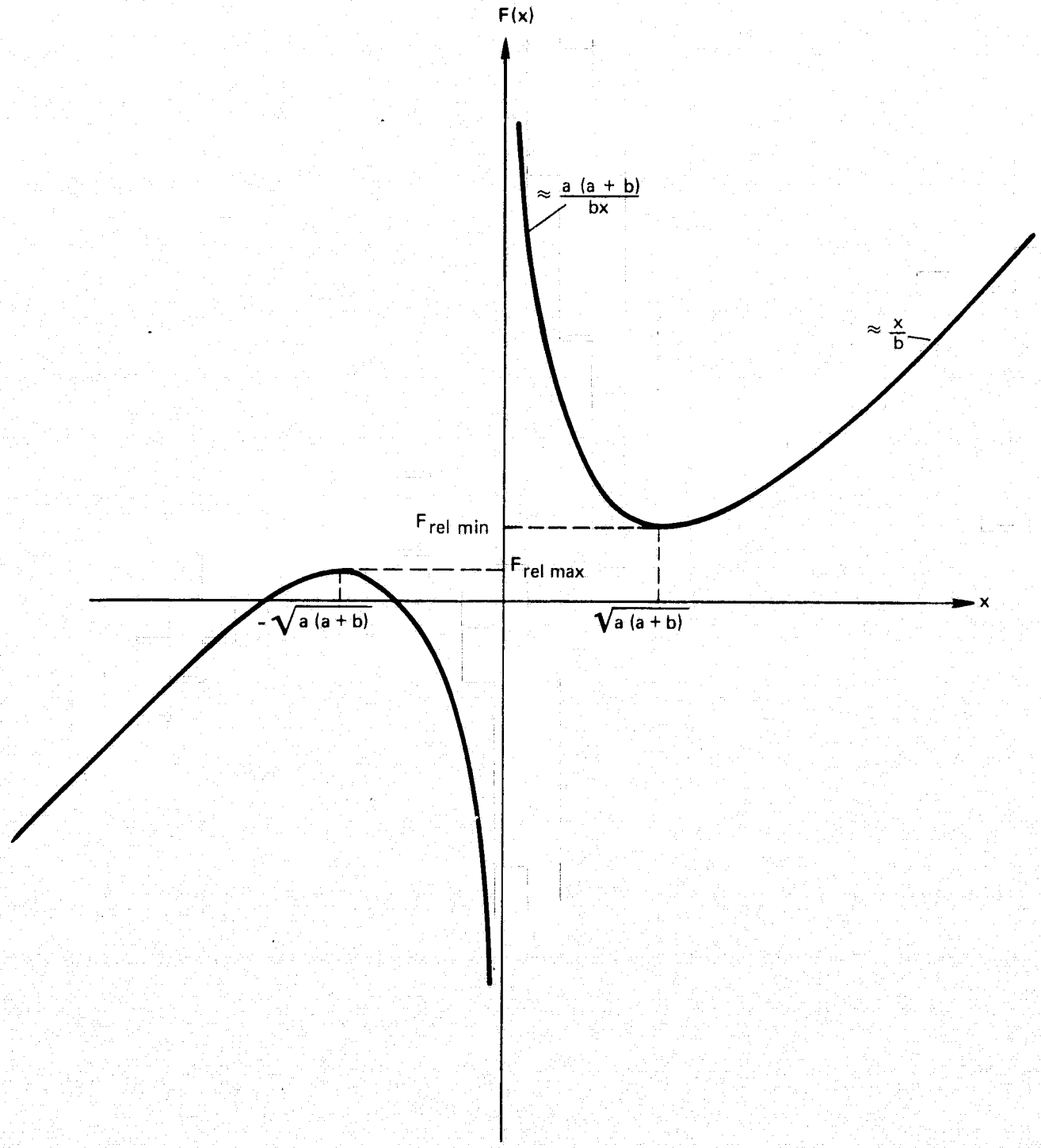

Fig. A-2 Plot of Relative Noise Figure as a Function of Source Resistance.

The result is

$$F_{min} = 1 + \frac{2}{b}\left[a + \sqrt{a(a+b)}\right] \qquad \text{(A-13)}$$

For completeness, the value of F corresponding to the negative value of x_o is given by

$$F_{rel\ max} = 1 + \frac{2}{b}\left[a - \sqrt{a(a+b)}\right] \qquad \text{(A-14)}$$

which is a relative maximum as seen in Fig. A-2.

If an attempt is made to minimize F with respect to a or b while holding the remaining two parameters constant, conditions are obtained which are not physically realizable. However, the results show that if x and b are fixed, then a should be as small as possible, while, if x and a are fixed, b should be as large as possible.

It is illuminating to compute the relative noise figure for the coupling network used with the viscous integrator (VI-293), for which

$$R_s \approx 160\Omega$$
$$R_1 \approx 4{,}600\Omega$$
$$R_2 \approx 25{,}000\Omega$$

Substitution of these element values in Eq (A-11) yields:

$$F_{actual} = \frac{(R_s + R_1 + R_2)(R_s + R_1)}{R_2 R_s} = \frac{(0.16 + 4.6 + 25)(0.16 + 4.6)}{(25)(0.16)} = 35.2 \qquad \text{(A-15)}$$

The optimum value of R_s is given by

$$R_{s\ optimum} = \sqrt{R_1(R_1 + R_2)} = \sqrt{4.6(29.6)} = 11.7\,K \qquad \text{(A-16)}$$

for which the corresponding value of F is computed below.

$$F_{min} = 1 + \frac{2}{R_2}\left[R_1 + \sqrt{R_1(R_1 + R_2)}\right] = 1 + \frac{2}{25}(4.6 + 11.7) = 2.3 \qquad \text{(A-17)}$$

It is seen that the relative noise figure can be improved by a factor of 15 by increasing R_s from 160 Ω to 11.7 KΩ.

The theory indicates that the signal generator resistance should be increased. However, inserting an additional resistor in series with the signal generator is not recommended as a solution in spite of the fact that doing so will minimize the relative noise figure F. The reason that adding a series resistor minimizes F is explained by the fact that F is a relative noise figure; it indicates the noisiness of a network (amplifier) relative to the noisiness of the source. Clearly, from the definition of noise figure (see Eq (A-6)), one can cause F to approach unity as closely as desired just by adding extra noise in the source. This approach makes the source so noisy that in comparison, the amplifier appears almost noise free. Therefore, inserting additional resistance causes the output signal-to-noise ratio to decrease, (see Eq (A-3)) the opposite of what is desired. This problem can be circumvented in two ways, described below.

One would like to keep the input signal-to-noise ratio constant while causing the apparent source resistance to increase. This can be accomplished with a good quality step-up transformer; the transformer increases the level of the input noise and input signal simultaneously, thus preserving the input signal-to-noise ratio, but it allows the transformation of impedance levels.

The increased noise at the source due to the reflected impedance makes the coupling network (amplifier) appear less noisy without deteriorating the signal-to-noise ratio at the input. Consequently, F, the relative noise figure is reduced and the output signal-to-noise ratio improves. The step-up transformer circuit is shown in Fig. A-3 below.

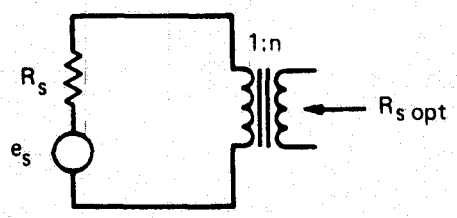

Fig. A-3 Circuit Model of Step-up Transformer.

The impedance transformation effected by the step-up transformer is expressed by

$$R_{s\,opt} = n^2 R_s \qquad \text{(A-18)}$$

where

$R_{s\ opt}$ = desired source resistance

R_s = actual source resistance

n = transformer turns ratio

For the example values previously cited, a step-up transformer with the following turns ratio is required.

$$n = \sqrt{\frac{R_{s\ opt}}{R_s}} = \sqrt{\frac{11.7\ K\Omega}{0.160\ K\Omega}} \qquad \text{(A-19)}$$

$$n \simeq 8.5$$

This technique is not without drawbacks. The effect upon other signal generator characteristics (e.g., elastic restraint torque) must be examined. The price paid in the noise figure improvement is that the transformer will "load down" the signal generator to a greater degree than in the absence of the transformer. That is, the impedance seen by the signal generator with the transformer in place is given by $\frac{1}{n^2} Z_{in}$, where Z_{in} represents the input impedance of the coupling network. Consequently, additional current is required to flow in the signal generator itself. The flow of current in the signal generator is a source of elastic restraint torque in the gyro and is generally undesirable. Additional current flow accentuates this effect. Therefore, one must take into account the relative importance of elastic restraint torque and improvement of noise figure. Careful evaluation must be made for a given application because noise figure improvement is proportional to $\frac{1}{n^2}$ for $R_s << R_{s\ opt}$, while the elastic restraint torque increases in proportion to n^2.

An alternate solution is to increase the number of turns in the signal generator windings, which increases the source resistance as well as the signal sensitivity (in the same ratio, except for slight geometric winding effects which may be neglected in our application). However, this requires additional room in which to place the extra wire. Instrument size constraints may preclude this additional space requirement. Employing finer wire to satisfy space allocations and noise figure improvement taxes the ability of the fabricator to wind wires of size # 36 and smaller in a space which is already tightly packed.

A more practical solution lies in the area of amplifier design. That is, design the input stage of the amplifier so that Eq (A-12) is satisfied with a given signal generator source resistance. Subsequent analysis and experiments should reveal whether this can be achieved and still be consistent with other engineering constraints imposed on the amplifier, e.g., power requirements, heat flow, regulation, etc.

It is important to remember that the result expressed by Eq (A-12) is based on an approximate thermal noise analysis. Consequently, experimental validation was undertaken. The results are presented in Part II of this Appendix, which follows.

Part II Experimental Results

There are several methods for measuring the relative noise figure F. A good account of these may be found in Ref 10. The method employed in our case is referred to as the "single frequency signal generator method". The instruments required are a signal generator, bandpass filter and a sensitive voltmeter. The circuit for which measurements were taken is shown below in Fig. A-4. The element values were chosen to yield a gain of 10^3, sufficient to amplify noise processes to levels which the voltmeter would sense.

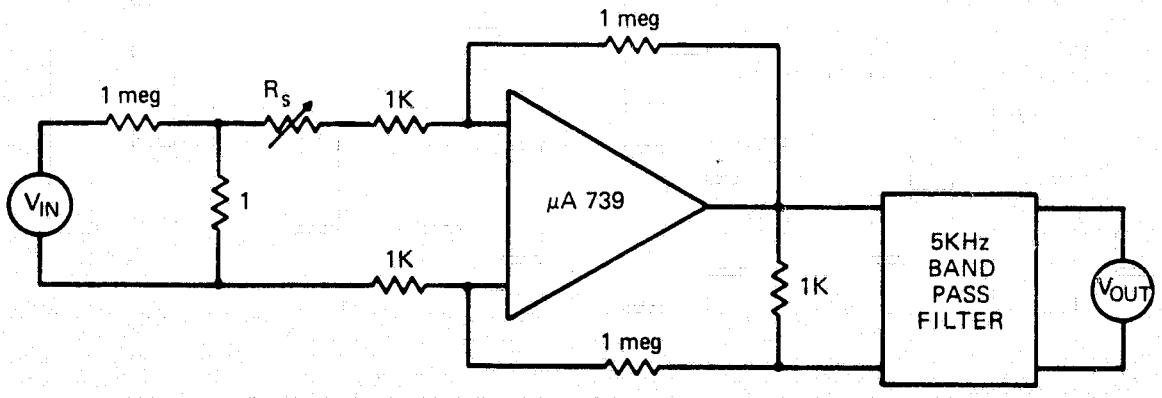

Fig. A-4 Circuit for Noise Figure Measurements.

Data was taken for nine values of R_s. Corresponding values of F were computed, the results of which are presented in the graph below.

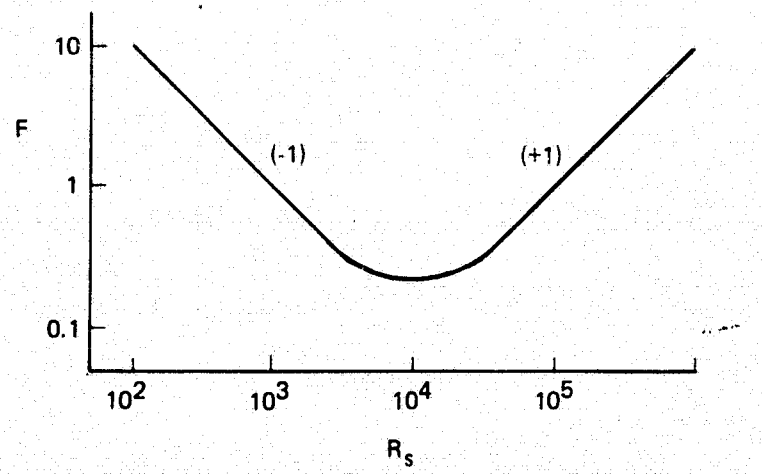

Fig. A-5 Noise Figure as a Function of Source Resistance.

Note that a broad minimum is present in Fig. A-5 indicating that for R_s taking on values in the range from 2k to 15k, F is minimized for all practical purposes. The shape of the curve for the data plotted clearly shows a minus one slope for $R_s < R_{opt}$ and a plus one slope for $R_s > R_{opt}$. This is consistent with Eq (A-11) for R_s satisfying the inequalities above. The absolute value of F was not properly scaled at the time the experiment was performed; consequently, F assumes values less than unity, a result known to be physically unrealizable. However, this is of no consequence because it was desired to establish the presence or absence of a minimum for F satisfying the problem constraints. The data validates the model for the coupling network, and for the circuit tested reveals that a factor of 30 improvement is possible in the relative noise figure when R_s is increased from 100 Ω to 10K Ω. Additional investigation is suggested to examine the tradeoffs between undesirable restraint torque and improvement in the signal to noise ratio. In order that optimum signal-to-noise ratios may be achieved, additional work is indicated in amplifier design. In this way, other noise sources within the gyro itself may be isolated and identified.

APPENDIX B

A LINEAR DISTRIBUTED SYSTEM WHOSE AGGREGATE POWER TRANSFER FUNCTION EXHIBITS A MINUS ONE SLOPE

It was suggested in Section 6 that linear time-invariant, distributed systems can give rise to power transfer functions proportional to $(1/\omega)$ over limited ranges of frequencies. A simple example which illustrates this behavior is shown below.

Consider a linear distributed system consisting of a group of first-order networks whose time constants (τ_i) are not all identical:

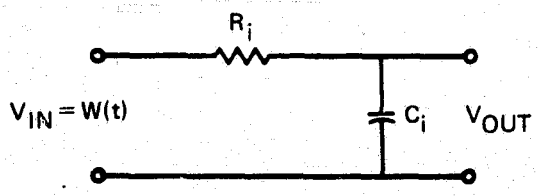

$$H(\tau, s) = \frac{1}{1 + s\tau_i}$$

$$\tau_i = R_i C_i$$

Let each of the first order networks be driven by its own white noise source. Assume that these noise sources are statistically independent. Also, let the power spectral density of the input to each of the filters be equal to K/N for all frequencies, where N is the number of filters in the distributed system. The power spectral density of the output of each of the filters will be equal to

$$PSD_{V_{out}} = \frac{K}{N}\left[H(j\omega, \tau_i)\, H(-j\omega, \tau_i)\right] \qquad \text{(B-1)}$$

where $H(j\omega, \tau_i)$ is the transfer function of the i^{th} filter with $s = j\omega$.

Consider the case where the filters in the distributed system have time constants distributed in such a manner that the number of filters with time constants between (τ) and $(\tau+d\tau)$ is given by $Np_{\tau_i}(\tau)\,d\tau$, where:

$$Np_{\tau_i}(\tau)\,d\tau = \begin{cases} N\left(\frac{1}{b-a}\right)d\tau & a \leqq \tau \leqq b \\ 0 & \text{elsewhere} \end{cases} \qquad \text{(B-2)}$$

As a consequence of the assumption that the N white noise sources are statistically independent, the power spectral density of the output of the distributed system is equal to the sum of the power spectral densities of the outputs of the individual filters. This sum will be referred to as the 'aggregate power transfer function'.

Allowing the distribution of time constants in Eq (B-2) to approach a continuum and combining Eq (B-1) and (B-2) yields:

$$PSD_{SYSTEM} = \int_a^b \left(\frac{K}{N}\left[H(\tau, j\omega)\,H(\tau, -j\omega)\right]\right)N\left(\frac{1}{b-a}\right)d\tau \qquad \text{(B-3)}$$

Substituting for $H(\tau, j\omega)$ we obtain

$$PSD_{SYSTEM} = \frac{K}{b-a}\int_a^b \frac{1}{1+\tau^2\omega^2}\,d\tau \qquad \text{(B-4)}$$

Performing the integration yields the result expressed by Eq (B-5):

$$PSD_{SYSTEM} = \frac{K}{(b-a)\omega}\left[\tan^{-1}(b\omega) - \tan^{-1}(a\omega)\right] \qquad \text{(B-5)}$$

The form of Eq (B-5) may be simplified by employing the trigonometric identity below.

$$\tan^{-1} A - \tan^{-1} B = \tan^{-1}\left[\frac{A-B}{1+AB}\right] \qquad \text{(B-6)}$$

The result is

$$PSD_{SYSTEM} = \frac{K}{(b-a)\omega}\tan^{-1}\left[\frac{\frac{1}{\omega}(b-a)}{\frac{1}{\omega^2}+ab}\right] \qquad \text{(B-7)}$$

A graph of this power spectral density in log-log coordinates is depicted below. Notice that the PSD is proportional to $(1/\omega)^*$ between the angular frequencies $1/b$ and $1/a$. This phenomenon is never observed in power transfer functions characterizing linear, lumped, time-invariant systems. As $b \to a$, the region in which the minus one slope exists gradually shrinks, yielding in the limit a PSD predicted by assuming that the time constants τ_i are all equal, with value a. Results similar to those derived here (that is, the occurrence of the minus one slope) are expected when other physically admissible distribution functions for the τ_i are assumed.

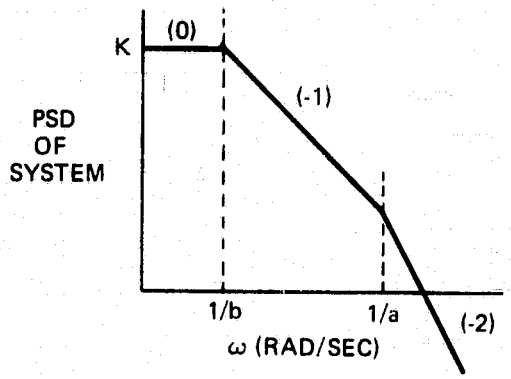

*For simplicity, the term "minus one slope" is used to describe a region in which the PSD on log-log paper is proportional to $\left(\frac{1}{\omega}\right)$.

APPENDIX C

HELPFUL HINTS FOR IMPLEMENTING POWER SPECTRAL DENSITY CALCULATIONS

The foundation of the frequency analysis of periodic signals was laid in 1807 by Fourier, who solved many problems in vibration and heat flow. Frequency analysis of aperiodic signals (transients) developed later. Historically, interest in random processes developed still later. These random processes which in a sense, bridge the gap between periodic and aperiodic signals, may be analyzed in terms of power spectral density - a concept derived by Norbert Wiener and others. The mathematical theory of power spectral density may be developed in a concise and straightforward manner. However, practical implementation requires clear understanding of the theory and a great appreciation for details. In the course of generating the PSD plots presented in this report, the authors gained experience which should prove beneficial to others engaged in similar ventures.

It is not intended to discuss the theory of power spectral density here; ample material on the subject is available in many excellent textbooks and papers. Rather, we would like to point out those areas in which subtle mistakes can, and did, occur when implementing the necessary mathematical methods on a digital computer.

It is usually desired to present PSD information (units^2/Hz) as a function of frequency (Hz). However, the literature abounds with mathematical development in terms of radian frequency. When meaningful numbers are desired, the 2π factor that relates angular frequency to frequency in Hz is of great importance. One enterprising engineer has aptly described the problem: Two pi or knot to pi - what is the variance ? We recommend that strict attention be paid to account for necessary factors of 2π.

The Fast Fourier Transform, the accepted method for efficiently computing power spectral density from a finite time series, is a very powerful tool in the hands of an experienced analyst. However, it does have limitations and they must be recognized. One should be aware of the fact that the Fast Fourier Transform can not tell us anything about the power present at zero frequency in the analysis of a realizable time series, that is, and infinitely long record of data would be required to yield information at zero frequency. The finite length of real data records constrain the lowest frequency at which power spectral density may be calculated.

On the other hand, the rate at which data is sampled constrains the highest frequency at which spectral information may be computed.

Before test results of interest are calculated, it is most illuminating to compute the PSD of signals whose spectral content is known. Our experience has shown that four such signals will most likely provide the means to debug an FFT computer program. They fall in two categories, deterministic and stochastic. The deterministic signals are a single sine wave and a square wave. The stochastic signals are computer-generated white noise, and exponentially-correlated noise (1^{st} order Markov process). These signals will aid in establishing that factors of 2 or 2π are not erroneously included in the computer program, since their PSDs are known and can be computed analytically in a straightforward manner. One should be careful when analyzing results obtained when discrete harmonics are used, since a PSD plot can not portray an impulse (with infinite height) in frequency. Rather observe that the area under the "triangle", or apparent spike, is to be interpreted as the power contained in a sine wave.

Another potential problem area lies in the use of the so-called Hanning filter. Specifically, when a Hanning filter symmetrical in time is analyzed, the corresponding weighting coefficients in frequency are found to be 1/4, 1/2, 1/4. However, real data usually starts at time t = 0 and ends at time t = T. Consequentially, a nonsymmetrical Hanning filter must be employed to accommodate real data. Analysis of this filter yields weighting coefficients of -1/4, 1/2, -1/4. This weighting is used in practice. Nonetheless, shift in the time origin discussed above can cause confusion.

We have found that the best way to present PSD information is on a log-log scale. This type of presentation establishes the basis for all discussions of slopes of asymptotes in this report. Unless some specialized need indicates otherwise, we recommend that all PSD plots be given on log-log cordinates. There is some freedom in averaging the "bunched-up" data on a log scale. Our approach to this averaging process is described in detail in Section 4.

The reader is cautioned not to read more into a PSD plot than is already there; that is, one PSD plot does not necessarily tell the whole story. Ideally, PSD calculations should be repeated for several distinct records of data obtained from a particular process. Uniformity of the resultant PSD plots then assures the stationarity of the process over the entire test time.

It is important to remember that PSD is a powerful tool but that it must be handled carefully.

APPENDIX D

SEISMIC CONSIDERATIONS

In order to obtain drift data that truly reflects random processes occurring within a gyro, a benign, motion-free test environment is required. This is true because ground motion (random or otherwise) will be sensed by the gyro, a measure of which will appear in its output signal. In practice it is not possible to establish a perfectly motionless test stand, since ultimately the ground serves as a support.

It is desirable, therefore, to test gyros in an environment that may be considered "quiet". By this it is meant that ground motion does not contribute significantly to the output of the gyro under investigation. One then is faced with the problem of deciding if a given test location is "quiet" relative to a specific sensor. But this requires knowledge of the ground motion at a test site as well as information concerning the magnitude of noise processes within the instrument. Because little reliable spectral information on ground motion is available in the frequency range of 0.01 Hz to 100 Hz, an apparent conflict results. That is, the test engineer must know the answer (spectral information on ground motion and gyro noise processes) before he can find the answer. In the absence of sufficiently sensitive instruments which generate no internal noise, the problem described above can only be resolved approximately. To illustrate, the gyro may be tested with its wheel on and then off. With the wheel on, ground motion is sensed and the PSD of its output would reflect its presence, but with the wheel off, ground motion (due to rotation about the input axis) would not be sensed. Differences in the two power spectral density plots would reflect ground motion and, of course, any effects due to wheel operation. This type of testing is an aid to assess the importance of ground motion. However, it is not aesthetically pleasing because with the wheel off, the gyro is not being tested in the manner in which it is used in practice and hence, is really a "different" instrument.

An alternate method for assessing the effect of ground motion is to test two "identical" gyros on the same stand with their input axes antiparallel. This allows cancellation of ground motion effects (assuming equal transfer characteristics) and would yield the behavior of the combination. While this does not reveal details about the ground motion per se, it allows qualitative assessment of gross effects by comparing

test results with those obtained by monitoring a single gyro whose output reflects the ground motion. Refined estimates of the spectral content of the noise processes within gyros will only become available as more is learned about the environment in which the sensors are tested. The authors anticipate that such information will also help to increase understanding of weather, earthquakes, and perhaps ecological phenomena. This may be done by compiling records of the power spectral density of ground motion over long periods of time. For the purpose of characterization of the spectral content of random processes within gyros, additional tests should be performed and long-term data records compiled.

REFERENCES

1. Hunter, L., Handbook of Semiconductor Electronics, 2nd edition, McGraw-Hill, 1962.
2. Jantsch, O., A Theory of 1/f Noise at Semiconductor Surfaces -- Solid State Electronics, Pergamon Press, Vol II, 1967. pp. 267-272.
3. Bendat, J. and Piersol, A., Random Data: Analysis and Measurement Procedures, Wiley Interscience, 1971, p. 146.
4. Cheng, D.K., Analysis of Linear Systems, Addison-Wesley, 1959.
5. McCarthy, F.D., Analysis of Drift, E-2298 Vol I, C.S. Draper Laboratory, MIT, July 1968.
6. Kraus, G.M., Gyro Noise Study, 21367-FR, Honeywell Inc, March 1970.
7. Rader, C.M., and Gold, B., Digital Processing of Signals, McGraw-Hill, 1969.
8. Jenkens, G.M., and Watts, D.G., Spectral Analysis and its Applications, Holden-Day, 1968.
9. Blackman, R.B., and Tukey, J.W., The Measurement of Power Spectra, Dover Publications, 1968.
10. Terman, F.E., and Pettit, J.M. Electronic Measurements, 2nd edition, McGraw-Hill, 1952.
11. Carlson, A.B., Communication Systems; An Introduction to Signals and Noise in Electrical Communication, McGraw-Hill, 1968. p. 431.